

Contents lists available at ScienceDirect

Petroleum Science

journal homepage: www.keaipublishing.com/en/journals/petroleum-science



Original Paper

Geophysical prediction of organic matter abundance in source rocks based on geochemical analysis: A case study of southwestern Bozhong Sag, Bohai Sea, China



Xiang Wang ^{a, b}, Guang-Di Liu ^{a, b, *}, Xiao-Lin Wang ^{a, b}, Jin-Feng Ma ^{c, d, **}, Zhen-Liang Wang ^{c, d}, Fei-Long Wang ^{c, d, e}, Ze-Zhang Song ^{a, b}, Chang-Yu Fan ^{c, d}

- ^a State Key Laboratory of Petroleum Resources and Prospecting, China University of Petroleum (Beijing), Beijing, 102249, China
- ^b College of Geosciences, China University of Petroleum (Beijing), Beijing, 102249, China
- ^c State Key Laboratory of Continental Dynamics, Northwest University, Xi'an, 710069, Shaanxi, China
- ^d Department of Geology, Northwest University, Xi'an, 710069, Shaanxi, China
- ^e CNOOC Tianjin Branch Company, Tianjin, 300459, China

ARTICLE INFO

Article history: Received 9 January 2023 Received in revised form 12 July 2023 Accepted 5 September 2023 Available online 9 September 2023

Edited by Jie Hao and Teng Zhu

Keywords:
Total organic carbon (TOC)
Residual hydrocarbon generation potential
(S2)
Geophysical prediction
Seismic attribute
Bozhong Sag
Bohai Bay Basin

ABSTRACT

The Bozhong Sag is the largest petroliferous sag in the Bohai Bay Basin, and the source rocks of Paleogene Dongying and Shahejie Formations were buried deeply. Most of the drillings were located at the structural high, and there were few wells that met good quality source rocks, so it is difficult to evaluate the source rocks in the study area precisely by geochemical analysis only. Based on the Rock-Eval pyrolysis, total organic carbon (TOC) testing, the organic matter (OM) abundance of Paleogene source rocks in the southwestern Bozhong Sag were evaluated, including the lower of second member of Dongying Formation $(E_3d_2^{\dagger})$, the third member of Dongying Formation (E_3d_3) , the first and second members of Shahejie Formation ($E_{2}s_{1+2}$), the third member of Shahejie Formation ($E_{2}s_{3}$). The results indicate that the E₂s₁₊₂ and E₂s₃ have better hydrocarbon generative potentials with the highest OM abundance, the E₃d₃ are of the second good quality, and the $E_3d_2^1$ have poor to fair hydrocarbon generative potential. Furthermore, the well logs were applied to predict TOC and residual hydrocarbon generation potential (S₂) based on the sedimentary facies classification, using $\Delta log R$, generalized $\Delta log R$, logging multiple linear regression and BP neural network methods. The various methods were compared, and the BP neural network method have relatively better prediction accuracy. Based on the pre-stack simultaneous inversion (P-wave impedance, P-wave velocity and density inversion results) and the post-stack seismic attributes, the three-dimensional (3D) seismic prediction of TOC and S2 was carried out. The results show that the seismic near well prediction results of TOC and S2 based on seismic multi-attributes analysis correspond well with the results of well logging methods, and the plane prediction results are identical with the sedimentary facies map in the study area. The TOC and S2 values of E2S1+2 and E2S3 are higher than those in E₃d₃ and E₃d₂, basically consistent with the geochemical analysis results. This method makes up the deficiency of geochemical methods, establishing the connection between geophysical information and geochemical data, and it is helpful to the 3D quantitative prediction and the evaluation of high-quality source rocks in the areas where the drillings are limited.

© 2023 The Authors. Publishing services by Elsevier B.V. on behalf of KeAi Communications Co. Ltd. This is an open access article under the CC BY-NC-ND license (http://creativecommons.org/licenses/by-nc-nd/4.0/).

1. Introduction

Organic matter (OM) abundance is a significant part of source rocks evaluation (Tissot et al., 1987; 1987). Although the traditional geochemical tests are accurate enough, it is also difficult to obtain three-dimensional (3D) distribution of source rocks and petroleum resource prediction in the areas with few drillings and samples.

^{*} Corresponding author.

^{**} Corresponding author. E-mail addresses: lgd@cup.edu.cn (G.-D. Liu), jfma@nwu.edu.cn (J.-F. Ma).

Geophysical methods are also significant for the research of source rocks, the well logs and seismic data are important supplements to the geochemical testing (Passey et al., 1990; Magoon and Dow, 1991; Zhu and Jin, 2002; Zhang and Zhu, 2007; Løseth et al., 2011).

Well logging is widely used in the petroleum exploration with high vertical resolution. Researchers have already started to identify source rocks using well logs such as natural gamma ray (GR). sonic transit time (DT), density (DEN) and resistivity (RD) logs (Beers, 1945; Swanson, 1960; Schmoker and Hester, 1981, 1983; Meyer and Nederlof, 1984; Herron, 1988). Total organic carbon (TOC) is one of the significant parameters of OM abundance. The common method for TOC prediction is $\Delta log R$ method, which is a quantitative evaluation model based on resistivity, porosity logs (generally DT) and thermal maturity parameter (LOM). It can be applied to terrestrial and marine source rocks, in which the resistivity logs mainly identify hydrocarbons in the pores of source rocks, and the porosity logs are mainly used to identify the solid kerogen (Passey et al., 1990; Kenomore et al., 2017; Sêco et al., 2019; Aziz et al., 2020; Tenaglia et al., 2020). Scholars have proposed various improved ΔlogR methods (Liu et al., 2014, 2021; Hu et al., 2015; Wang et al., 2016; Zhao et al., 2016; Zhu et al., 2019). Logging multiple linear regression method is also a popular method to predict the TOC. The well logs have high correlation coefficients with TOC are selected and then the multiple linear regression method is used to calculate the TOC. However, this method has regional limitations and it is difficult to be popularized (Aziz et al., 2020).

Although well logs combined with geochemical data could evaluate the vertical heterogeneity of source rocks more accurately. the sparse well logs and geochemical data in areas with few drillings hinder 3D prediction of the source rocks. Therefore, additional research with seismic methods is needed. Previous studies mainly used post-stack seismic data to predict source rocks by combining the seismic facies and seismic attributes (Zhang and Zhu, 2007; Gupta et al., 2013; Infante-Paez et al., 2017). In general, the study of seismic response in source rocks should be based on the sequence stratigraphy method. After well-seismic calibration, picking up various seismic attributes (amplitude, frequency, phase, etc.), and performing single attribute correlation analysis with TOC curves, and then establishing mathematical model by selected seismic attributes with high correlation coefficients. Finally, the mathematical model obtained by training is applied to the 3D seismic data volume (Løseth et al., 2011; Li et al., 2014; Ji et al., 2018; Qin et al., 2018). Seismic inversion is also an extensive method to quantitatively evaluate OM abundance of source rocks (Chen, 2014; Badics et al., 2015; Tao et al., 2015; Wang et al., 2016; Infante-Paez et al., 2017; Niu et al., 2017; Chen et al., 2018; Chopra et al., 2018; Mahmood et al., 2018; Paris and Stewart, 2020; Sahoo et al., 2021). After petrophysical analysis, scholars found that there are good correlations between TOC and elastic parameters such as P-wave impedance and pre-stack density inversion results, so the TOC prediction can be calculated by post-stack or pre-stack seismic inversions. In recent years, the shale rock physics and pre-stack AVO analysis have become focused areas. Some published articles reported that source rocks have significant class IV AVO characteristics, that is, the intensity of negative reflection amplitude decreases with the increase of offset (Carcione et al., 2011; Løseth et al., 2011; Del Monte et al., 2018). Numerous studies on the petrophysics of organic-rich shale have been reported, which has laid foundation for the study of the relationship between kerogen and petrophysical elastic parameters of source rocks (Vernik and Nur, 1992; Vernik and Landis, 1996; Carcione, 2000; 2001, 2015; Hansen et al., 2019; Del Moro et al., 2020; Zhao et al., 2020; Matava et al., 2021).

In recent years, the application of neural network methods for

petroleum exploration are becoming very popular, so lots of models for predicting TOC by machine learning have also been proposed. Based on petrophysical analysis, several well logs have significant correlations with OM abundance were selected, and applied different machine learning algorithms to establish models for prediction (Huang and Williamson, 1996; Kamali and Mirshady, 2004; Bolandi et al., 2015; Tan et al., 2015; Verma et al., 2016; Ji et al., 2018; Wang and Peng, 2018; Shalaby et al., 2019; Wang et al., 2019; Zhao et al., 2021).

Researchers have conducted some geophysical studies for the source rocks of the Bohai Bay Basin. Based on geochemical characteristics, well logging and seismic data. Niu et al. (2017) used post-stack impedance inversion to predict the TOC of the Shahejie Formation source rocks in the Liaoxi Sag, Bohai Bay Basin. Cai et al. (2018) predicted TOC of Shahejie Formation source rocks in the Liaodong Sag of Bohai Bay Basin by using post-stack multi-attribute fusion method. Wang et al. (2019) proposed a six-layer convolutional neural network (CNN) method to predict TOC, S₁ and S₂ of Dongying Sag, Bohai Bay Basin. By modifying the model parameters, Liu et al. (2014, 2021) introduced the proportion coefficient K, which was considered to be an integrated reflection of kerogen, porosity and hydrocarbon components, proposed the variable overlay-coefficient $\Delta log R$ method (V- $\Delta log R$), and satisfactory prediction results have been obtained in Dongying and Zhanhua Sag, Bohai Bay Basin. In general, there were few geophysical studies for source rocks of Bozhong Sag, especially in the aspect of seismic research. In addition, the published articles were mainly based on post-stack seismic data, and there were few cases of using pre-stack seismic data to predict source rocks. Moreover, the pre-stack seismic data contain more reservoir information, and can describe the reservoirs and hydrocarbons more accurately, which contributes to more accurate evaluation of source rocks (Hampson et al., 2005; Sen and Stoffa, 2013; Zhao et al., 2021).

Based on organic geochemical analysis, this study compares multiple well logging methods, preferably BP neural network for prediction of TOC and S₂, and then combines seismic inversion (P-wave impedance, P-wave velocity, density inversion results) and seismic attributes to predict the 3D distribution of TOC and S₂. A geochemistry-logging-seismic workflow of terrestrial deep source rocks evaluation method is established in the southwestern Bozhong Sag of Bohai Bay Basin.

2. Geological settings

The Bohai Bay Basin is located in the eastern part of the North China Block, with an area of nearly $2 \times 10^5 \text{ km}^2$, including a land area of $1.2 \times 10^5 \text{ km}^2$, and it is a Cenozoic lacustrine pull-apart basin, which resulted in the disappearance of the Upper Cretaceous strata, denudation of the Mesozoic and Paleozoic sediments (Watson et al., 1987; Allen et al., 1997; Sun et al., 2008; Zhou et al., 2009; Feng et al., 2016; Yu et al., 2020; Fu et al., 2022). The Bozhong Sag is the largest hydrocarbon-rich Sag and the Cenozoic depositional center of the Bohai Bay Basin, covering an area of 8660 km², with a thick layer of Cenozoic deposition, surrounded by the Shijiutuo Uplift, Shaleitian Uplift, Chengbei Lower Uplift and Bonan Lower Uplift. A series of significant exploration discovery have been made in the Bozhong Sag, and several large and medium-sized oil and gas fields such as BZ19-4, PL19-3, BZ13-1 and CFD6-4 have been discovered (Xie et al., 2018; Yin et al., 2020; Yu et al., 2020). In recent years, the Tianjin Branch of CNOOC discovered a large gas field in the deep Archean metamorphic exposed-hill of the Bozhong 19-6 (BZ19-6) structure and a large oil field in Archean granite gneiss buried-hill oilfield of the Bozhong 13-2 (BZ13-2) in the southwestern Bozhong Sag (Shi et al., 2019, 2021; Xu et al., 2019; Xue et al., 2020; Yin et al., 2020; Li et al., 2021) (Fig. 1).

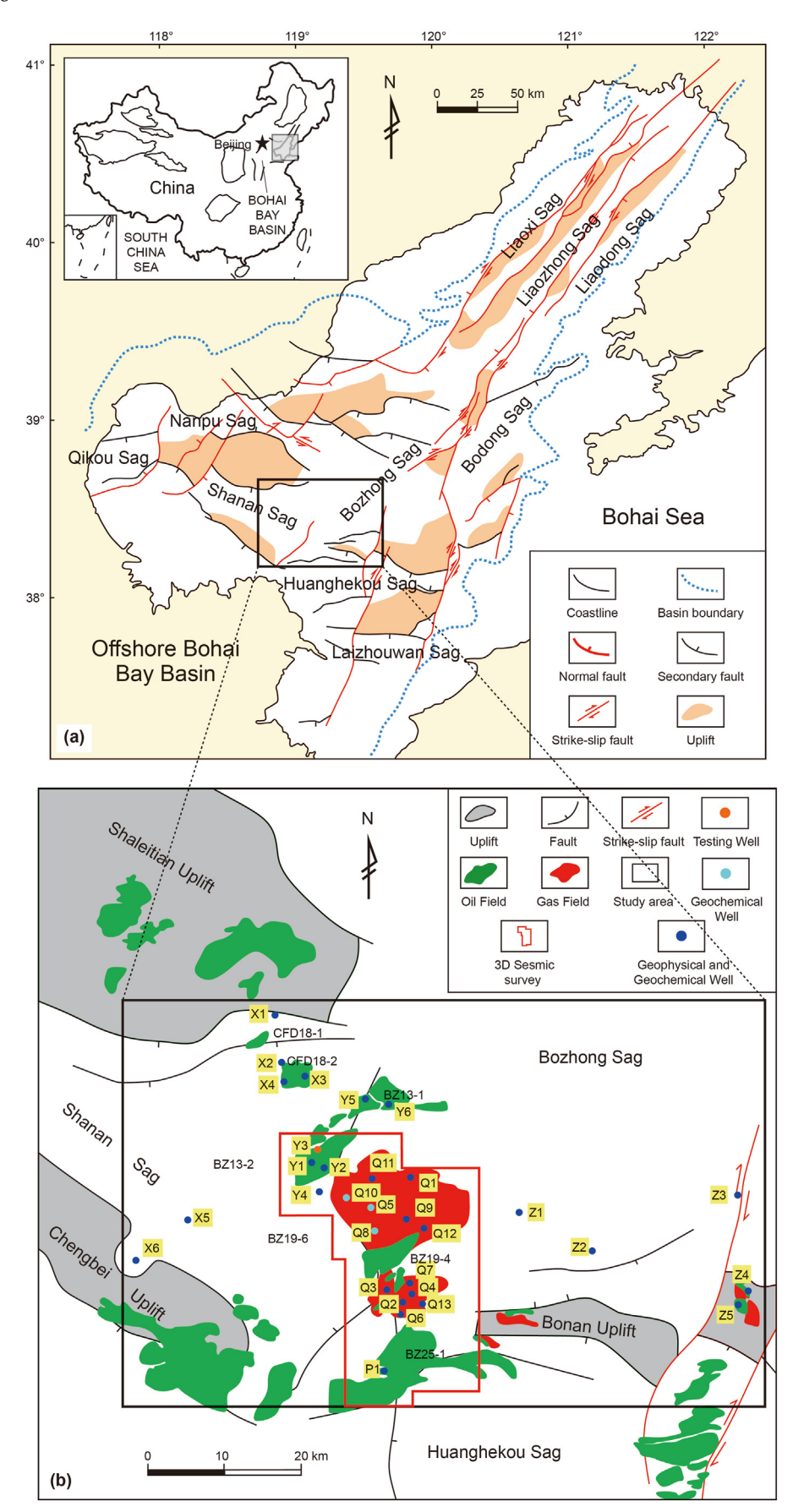


Fig. 1. (a) The location of the offshore Bohai Bay Basin (Feng et al., 2016; Fu et al., 2022). (b) Location map of southwest part of Bozhong Sag.

According to previous studies, the Bozhong Sag has experienced rifting and depressional periods since the Cenozoic, with relatively independent extensional and strike-slip fractures, and strike-slip is the main control factor for tectonic movement, trap formation and petroleum accumulation since its Cenozoic deposition (Qi et al., 1995a, 1995b; Feng et al., 2016; Wang et al., 2017; Xie et al., 2018; Yu et al., 2020). Researchers have extensively evaluated the source rocks in the Bohai Sea area, including four significant Paleogene source-rock intervals, namely: (1) the third member of the Shahejie Formation (E₂s₃), (2) the first and second members of the Shahejie Formation (E_2s_{1+2}) , (3) the third member of the Dongying Formation (E₃d₃) and (4) the lower second member of the Dongying Formation ($E_3d_2^L$). Previous studies have reported OM characteristics, hydrocarbon generation history, depositional environment based on organic biomarkers, stable carbon isotope and trace elements, the source rocks in Bozhong Sag were further studied (Li et al., 2001; Hao et al., 2010, 2011; Wang et al., 2015; Jiang et al., 2016, 2019; Yin et al., 2020; Chen et al., 2021). However, the lacustrine source rocks in Bozhong Sag have significant heterogeneity, and source rocks in different sub-sags may have different hydrocarbon generation potentials (Hao et al., 2010, 2011; Wang et al., 2022), and the studies on quantitative evaluation of source rocks in Bozhong sub-sags were insufficient. The source rocks of E₂s₃, which are the most important source rocks in Bozhong Sag, represent lacustrine, fan delta sedimentary facies. The thickness of E_2s_{1+2} source rocks are thinner than that of E_2s_3 , representing shore-shallow lacustrine, braid-delta and fan delta sedimentary facies. The sedimentary facies of E_3d_3 and $E_3d_2^L$ are river-delta and lacustrine sedimentary facies, and their contribution to petroleum accumulation in Bozhong Sag could not be ignored (Hao et al., 2010; Jiang et al., 2016) (Fig. 2).

3. Samples and methodology

In this study, the data of 31 wells (X1, X2, X3, X4, X5, X6, Y1, Y2, Y3, Y4, Y5, Y6, Q1, Q2, Q3, Q4, Q5, Q6, Q7, Q8, Q9, Q10, Q11, Q12, Q13, P1, Z1, Z2, Z3, Z4 and Z5), the pre-stack CRP gathers, post-stack seismic data and seismic horizons in the southwestern Bozhong Sag were collected, the 3D seismic survey covers approximately 800 km². A total of 718 mudstone samples were collected for TOC testing and Rock-Eval pyrolysis. The Rock-Eval pyrolysis and TOC data of several wells (Q4, Q11, X5, X6, Z1) have been reported, but they were used for research on organic facies, sedimentary environment of source rocks, and oil-source correlation. These data have not been used for geophysical prediction of source rocks (Wang et al., 2020, 2022; Yin et al., 2020). All the above experimental results were analyzed and identified in the Bohai experimental center of CNOOC, State Key Laboratory of Continental Dynamics of Northwest University, and State Key Laboratory of Petroleum Resources and Prospecting, China University of Petroleum. The logging data and seismic data were obtained from the Tianjin Branch of CNOOC.

3.1. Geochemical analysis and geophysical data

- 1) TOC analysis. TOC was tested using CS-230 carbon and sulfur analyzer. First, the mudstone samples were crushed to 80 mesh, weighed to take 0.3 g sample and put into a quartz crucible. Then 5% dilute hydrochloric acid was added and then it was heated at 80 °C to remove the inorganic carbon. The selected samples shall be washed with pure water and dried at 60 °C. Finally, the crucible in which the samples were placed in the CS230 carbon and sulfur analyzer to determine the TOC.
- 2) Rock-Eval pyrolysis. For Rock-Eval pyrolysis using ROCK EVAL 6 pyrolyzer, the mudstone samples were crushed to 100 mesh and

- then 60 mg of samples were weighed and heated for pyrolysis and placed in the Rock-Eval pyrolyzer.
- 3) The well logs mainly include sonic transit time (DT and DTS), P-wave (converted from DT), S-wave (converted from DTS), density (DEN), deep resistivity (RD) and natural gamma ray (GR). The wells involved in the logging prediction methods include: X1, X2, X3, X4, X5, X6, Y1, Y2, Y3, Y4, Y5, Y6, Q1, Q2, Q3, Q4, Q6, Q7, Q9, Q11, Q12, Q13, P1, Z1, Z2, Z3, Z4 and Z5.
- 4) Seismic data inline direction is north-south, crossline direction is east-west. Seismic bin size is 25 m × 12.5 m, the post-stack seismic data with the traditional processing of amplitude recovery and residual amplitude compensation, static correction, suppress multiple waves, velocity analysis, pre-stack time migration. For pre-stack simultaneous inversion, gather conditioning is needed. The wells involved in the seismic inversion and attributes analysis within the seismic workings include: Y1, Y2, Y4, Q1, Q2, Q3, Q4, Q6, Q7, Q9, Q11, Q12, Q13 and P1.

3.2. Well logging evaluation of organic matter abundance in source rocks

Generally, source rocks are mainly marine carbonate rocks or terrestrial lacustrine mudstones, which mainly consist of rock matrix and pores, and the rock matrix of non-source rocks are mainly clay minerals (montmorillonite, kaolinite, illite, etc.), nonclay minerals (quartz, feldspar, carbonate minerals, etc.) and kerogen, and as the source rocks mature, the solid kerogen will evolve into oil and gas entering the pore and drive out the pore water (Fig. 3). The rock physical differences (P-wave velocity, density, resistivity, etc.) between kerogen and other clastic particles (such as quartz, feldspar, and carbonate minerals) in source rocks are more significant, so the variability of component content (the OM abundance) of source rocks could be identified by well logging methods (Passey et al., 1990; Zhao et al., 2016).

A total of 620 groups data of TOC and S_2 of the southwestern Bozhong Sag were selected, including 312 groups in $E_3d_2^L$, 142 groups in E_3d_3 , 59 groups in E_2s_{1+2} , and 107 groups in E_2s_3 . Based on $\Delta logR$ method, generalized $\Delta logR$ method, multiple linear regression and BP neural network method, the determination coefficient R^2 and average relative errors of the prediction models in different intervals and sedimentary facies are compared. In order to select the suitable and unified method, the data of different intervals are unified together for comparison and optimization.

3.2.1. Adapting Passey et al. (1990) method to estimate TOC

The $\Delta log R$ method is one of the most classical logging prediction methods for estimating TOC proposed by Passey et al. (1990). The RD logs and the DT logs are superimposed in reverse in the nonsource rocks intervals, and the part where the two logs completely overlap in a certain range is the baseline. Since the sonic transit time value of kerogen is generally larger than that of inorganic minerals such as quartz and feldspar, the resistivity value of oil and gas is higher than inorganic-rich intervals, a certain separation between the baselines will be generated, and the separation is designated as $\Delta log R$, that is

$$\Delta \log R = \log_{10}(R/R_{\text{baseline}}) + 0.02 \times (\Delta t - \Delta t_{\text{baseline}})$$
 (1)

In Eq. (1), where R is the resistivity log value, $R_{\rm baseline}$ is deep resistivity baseline value, Δt is sonic transit time log value, $\Delta t_{\rm baseline}$ is sonic transit time baseline value, respectively. And the $\Delta \log R$ separation is linearly related to TOC values through the maturity parameter (LOM) in Eq. (2). In general, LOM can be obtained from a variety of laboratory analysis and testing, burial and thermal

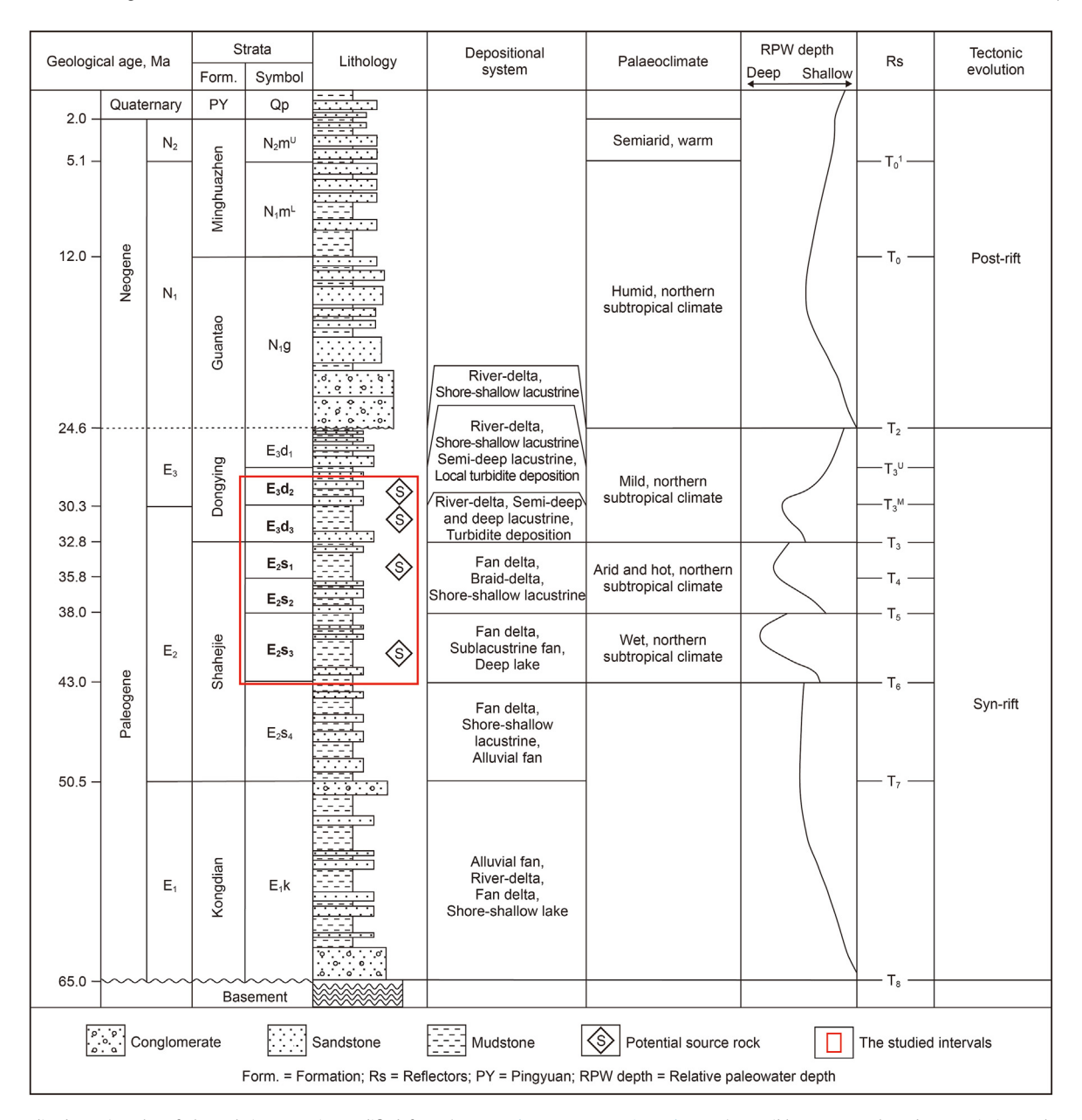


Fig. 2. Generalized stratigraphy of the Bohai Bay Basin modified from (Hao et al., 2010, 2011; Li et al., 2021). Possible source rock and reservoir intervals are marked. Form = Formation; PY = Pingyuan; RPW Depth = Relative paleo-water; Rs = Reflectors.

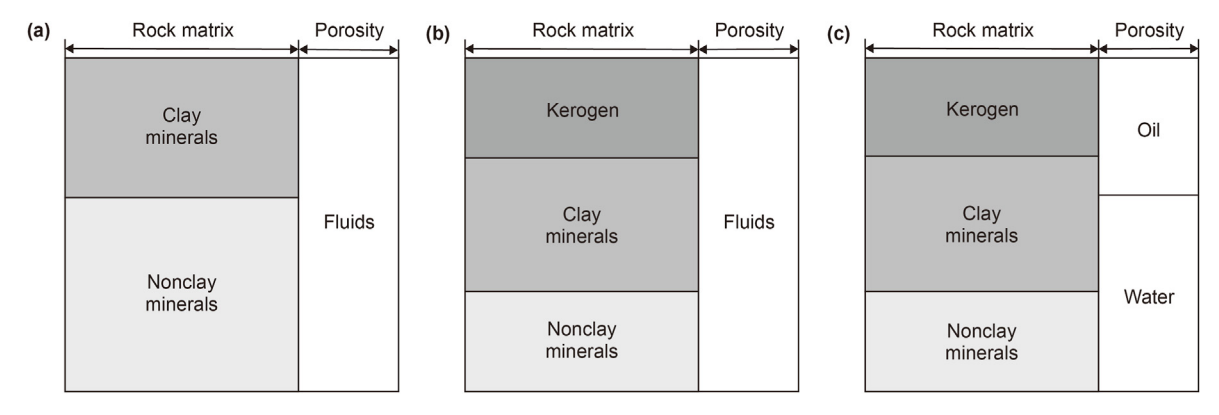


Fig. 3. Petrophysical models of non-source, immature and mature source rocks modified from (Passey et al., 1990; Zhao et al., 2016). (a) Non-source rocks model. (b) Immature source rocks. (c) Mature source rocks.

history. LOM determine the accuracy of TOC prediction.

$$TOC = (\Delta log R) \times 10^{(2.297 - 0.1688 \times LOM)} + \Delta TOC$$
 (2)

3.2.2. Adapting generalized ∆logR method to estimate TOC

The $\Delta logR$ method produced a more apparent amplitude difference between the RD and DT logs superimposed on the intervals of mature source rocks (Fig. 4), and the generalized $\Delta logR$ method is a method proposed by (Hu et al., 2015) for deep intensive compaction formations in the terrestrial facies, which takes into account that the relationship between TOC values and $\Delta logR$ is not a simple linear relationship, and needed to introduce LOM, but the conductive component of the terrestrial source rocks makes the separation of the immature source rocks intervals implicit to be calculated, thus introducing the GR log, which is more sensitive to the terrestrial intensive compaction formations, and this article also introduce the DEN log, which is sensitive to the OM. The generalized $\Delta logR$ method considering GR and DEN is obtained:

$$TOC = [a \times log_{10}(GR) + b \times DEN + c] \times \Delta logR + \Delta TOC$$
 (3)

where a, b, and c are fitting coefficients and Δ TOC is the background value of OM abundance, and Eq. (3) is used in combination with Eq. (1).

3.2.3. Adapting multiple linear regression to estimate TOC

Multiple linear regression method is also a popular method to calculate the OM abundance of source rocks. It was found that the correlations between logging parameters and OM abundance parameters (TOC and S_2) were inapparent, so the mathematical relationship between multiple logging parameters with TOC and S_2 could be considered for the prediction.

According to previous studies, the P-wave velocity of kerogen is generally 1700–2300 m/s, the P-wave velocity of clay minerals such as kaolinite and illite are generally 3000–4000 m/s, while the P-wave velocity of minerals such as quartz, feldspar and calcite is generally above 4000 m/s. Therefore, the OM in the source rocks would result in the decrease of the P-wave velocity (the increase of DT values) (Mavko et al., 2020). The density of kerogen is generally 1.3–1.4 g/cm³, while the density of other minerals such as quartz,

feldspar, calcite are higher than 2.0 g/cm³, therefore, the OM enrichment would result in the decrease of DEN values. Moreover, kerogen contains radioactive elements such as U, Th, K, etc., which will affect the RD and GR (Mavko G et al., 2020).

According to 3D cross-plot analysis (Fig. 5), it is found that the correlations of DT, DEN, RD and GR with TOC and S_2 decrease in southwestern Bozhong Sag. Therefore, the calculation formula of TOC and DT, DEN, RD and GR logs is established in Eq. (4), where d, e, f, g and h are fitting coefficients:

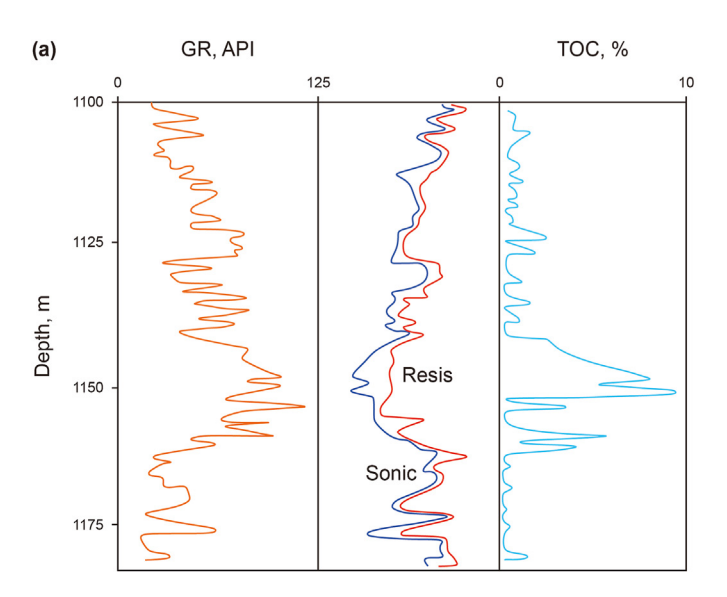
$$TOC = d \times DT + e \times DEN + f \times RD + g \times GR + h$$
 (4)

3.2.4. Adapting BP neural network method to estimate TOC

BP (back propagation) neural network is a multi-layer feedforward neural network trained according to the error back propagation algorithm. Its topology includes input layer, hidden layer and output layer (Fig. 6), and the core theory is that the training samples are input from the input layer, processed by multiple hidden layers and output to the output layer, if the desired output is not obtained, the hidden layers back propagate and pass the error signal to the neurons in the previous layer, and then adjust the weights and thresholds so that the error between the actual output and the desired output is minimized. This process is called back propagation (Huang and Williamson, 1996; Kamali and Mirshady, 2004; Bolandi et al., 2015; Tan et al., 2015; Verma et al., 2016; Ji et al., 2018; Wang et al., 2017; Shalaby et al., 2019; Wang et al., 2019; Zhao et al., 2021). To obtain the desired output results, the prediction of the network can be optimized by adjusting the number of layers of the hidden layer or increasing the number of neuron nodes in a single hidden layer. Only nonlinear separation problems require multiple hidden layers, and the neural network model with a single hidden layer can effectively approximate arbitrary continuous functions. In this study, the BP neural network model with a single hidden layer is constructed, and its mathematical formulas are as follows in Eqs. (5)–(8):

Input layer:

$$x^{(i)}$$
 (5) Hidden layer:



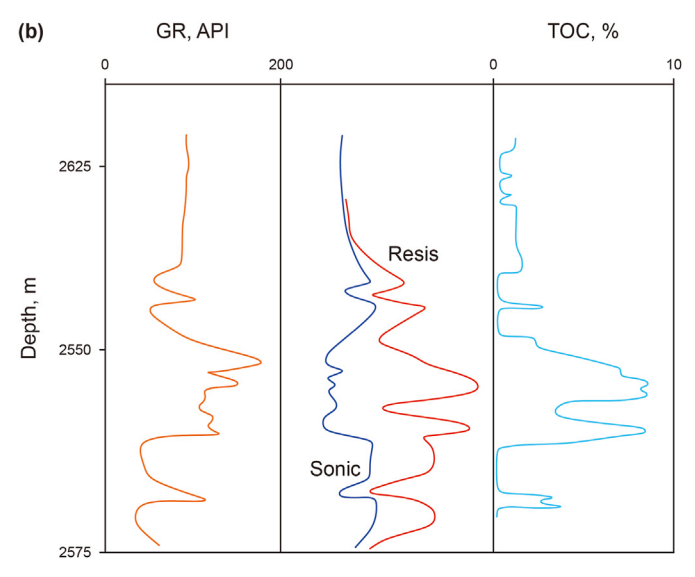


Fig. 4. (a) Sonic/resistivity overlay difference and calculated TOC profile of immature source rocks. (b) Sonic/resistivity overlay difference and calculated TOC profile of mature source rocks modified from (Passey et al., 1990; Hu et al., 2015).

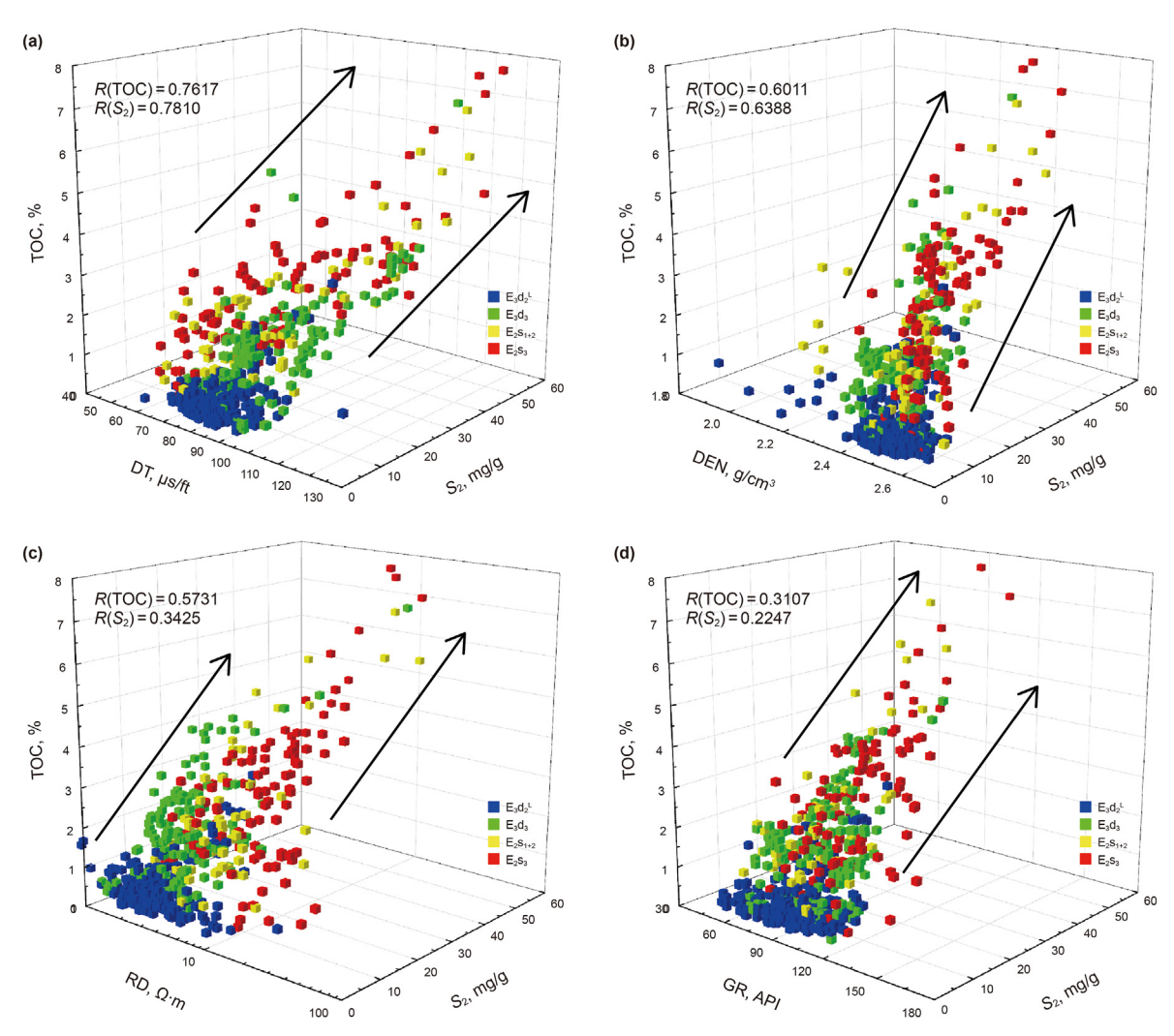


Fig. 5. Correlation analysis diagram between logging parameters and OM abundance (TOC and S2). (a) DT, (b) DEN, (c) RD, (d) GR.

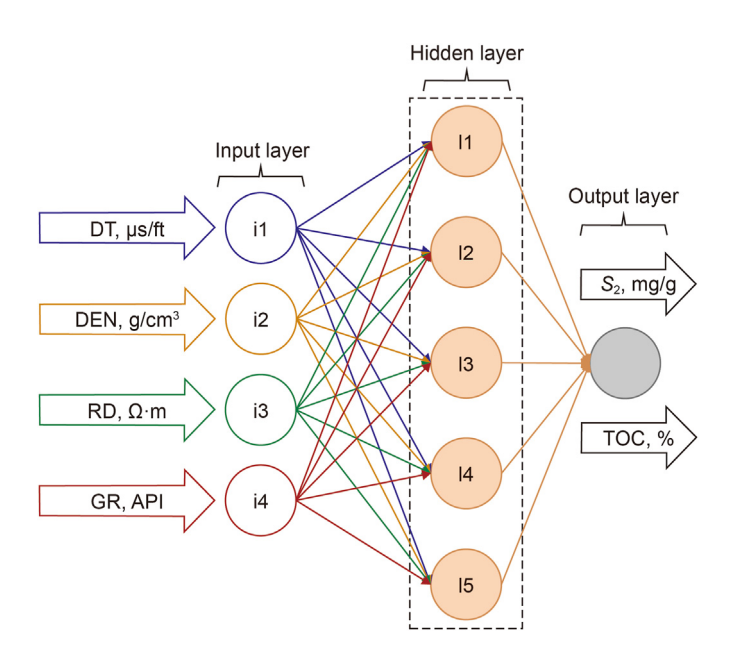


Fig. 6. Diagram indicates formulation of input petrophysical data to TOC and S_2 by a three layered artificial neural network modified from (Bolandi et al., 2015).

$$a_1^{(i)} = f(w_1 x^{(i)} + b_1) \tag{6}$$

Output layer:

$$\hat{y}^{(i)} = f\left(w_2 a_1^{(i)} + b_2\right) \tag{7}$$

The output expression after several training sessions is

$$Y = \sum_{j=1}^{m} \left[w_{2jk} \times f \left(\sum_{i=1}^{n} w_{1ij} \times x^{(i)} + b_{1j} \right) \right] + b_{2k}$$
 (8)

where $x^{(i)}$ is the feature vector of the output layer; $f(\cdot)$ is the activation function; w_{1ij} is the weight from the input layer to the hidden layer; b_{1j} is the threshold from the input layer to the hidden layer; w_{2jk} is the weight from the hidden layer to the output layer; b_{2k} is the threshold from the hidden layer to the output layer.

Similarly, chloroform bitumen "A", hydrocarbons formed before pyrolysis S_1 , S_2 and other OM abundance parameters can also be calculated by this method.

3.3. *Seismic prediction of organic matter abundance in source rocks*

3.3.1. Pre-stack simultaneous inversion

Based on the pre-stack CRP gathers, well logs data, geological data, etc., the pre-stack simultaneous inversion is performed (Hampson et al., 2005; Sen and Stoffa, 2013; Chen et al., 2018) (14 inversion wells, namely, Y1, Y2, Y4, Q1, Q2, Q3, Q4, Q6, Q7, Q9, Q11, Q12, Q13, P1), and after the gather conditioning processes, wavelet extraction, well seismic calibration, low frequency model establishment. The pre-stack inversion data results such as P-wave, density, S-wave, P-wave impedance, and P-wave and S-wave velocity ratios were obtained to provide the basis for multi-attributes prediction of TOC and S₂.

A. Pre-stack gather conditioning. The original seismic data is prestack CRP gathers, which has low signal-to-noise ratio, no flattening of the events, and large differences in wavelet morphology, etc. Therefore, to obtain more accurate inversion results, the original CRP gathers are needed gather conditioning before the prestack inversion. It can be seen that after pre-stack gather conditioning, the reflection horizons of the gathers are flattened and the signal-to-noise ratio and resolution are improved, which can be used for pre-stack simultaneous inversion and OM abundance prediction in the southwestern Bozhong Sag (Fig. 7).

B. Wavelet selection and generation of synthetic seismogram. After obtaining the CRP gathers by the pre-stack gather conditioning, it is necessary to perform well-seismic calibration by correlating well logs with the seismic data. In this work, we extract the zero-phase statistical wavelet to make synthetic seismogram. The synthetic seismogram is further calibrated and compared with the actual seismic traces near wells, and the corresponding horizons were traced and adjusted repeatedly with the aim of obtaining accurate and reliable time-depth relationships at the well locations. Fig. 8 shows the synthetic seismogram results of well Q2 and well Q3, with the geological strata on the far left, the P-wave velocity logs on the red curve, the density logs on the blue curve, and the blue seismic traces are the synthetic seismogram, red seismic traces are the seismic traces near wells, and the actual seismic traces near wells are shown on the far right. The yellow boxes at the top and bottom are the target intervals. It can be seen that the synthetic seismogram results in the target formations are satisfactory, with correlation coefficients of 0.8410 for well Q2 and 0.8020 for well Q3.

C. Establishment of low frequency model. After establishing the reliable seismic time-depth relationship, a low-frequency model needs to be built with the help of logging information (Mahmood et al., 2018). The pre-stack simultaneous inversion requires the establishment of the pre-stack P-wave impedance, the P-wave velocity and the density models to constrain the inversion results, filling the low-frequency portion of the seismic frequency spectrum.

D. Pre-stack simultaneous inversion results. The final inversion results were obtained through several inversion analyses and improvements. Fig. 9 shows the P-wave impedance, P-wave velocity and density inversion results (Inline 4938) over well Q7, the well position was inserted into the well logs, and its color bar and the inversion results color bar were adjusted to be consistent, the inversion results near wells correspond well with the well logs, so the inversion results have high credibility.

3.3.2. Multi-attributes fusion analysis based on neural network

Then multiple attributes of the seismic traces near wells are extracted and combined with the P-wave impedance, P-wave velocity and density inversion results to perform multi-attributes analysis with TOC and S_2 . The multi-attributes fusion prediction of several attributes has the highest correlation coefficients with TOC and S_2 are performed using the neural network method to obtain the TOC and S_2 prediction curves for the wells within the seismic data, and then the neural network-trained model is applied to the entire seismic data to obtain the TOC and S_2 3D prediction results.

According to the analysis of the previous well logging parameters cross-plots (Fig. 5), it is found that the OM abundance parameters (TOC, S_2) of source rocks had the highest correlation coefficients with DT and DEN logs, so this study uses the P-wave velocity, density and P-wave impedance inversion results combined with post-stack seismic data for multi-attributes optimization and analysis.

Next, we need to extract the seismic attributes near wells and make correlation analysis with the TOC and S_2 curves predicted by BP neural network method. Figs. 10 and 11 are the TOC and S_2 curves of Well Q2, Q3, Q4 and Q12, and the seismic traces near wells, P-wave impedance, P-wave velocity and density. In order to make a satisfying match between TOC/ S_2 curves and seismic attributes, it is necessary to time shift, smooth and filter logs (the

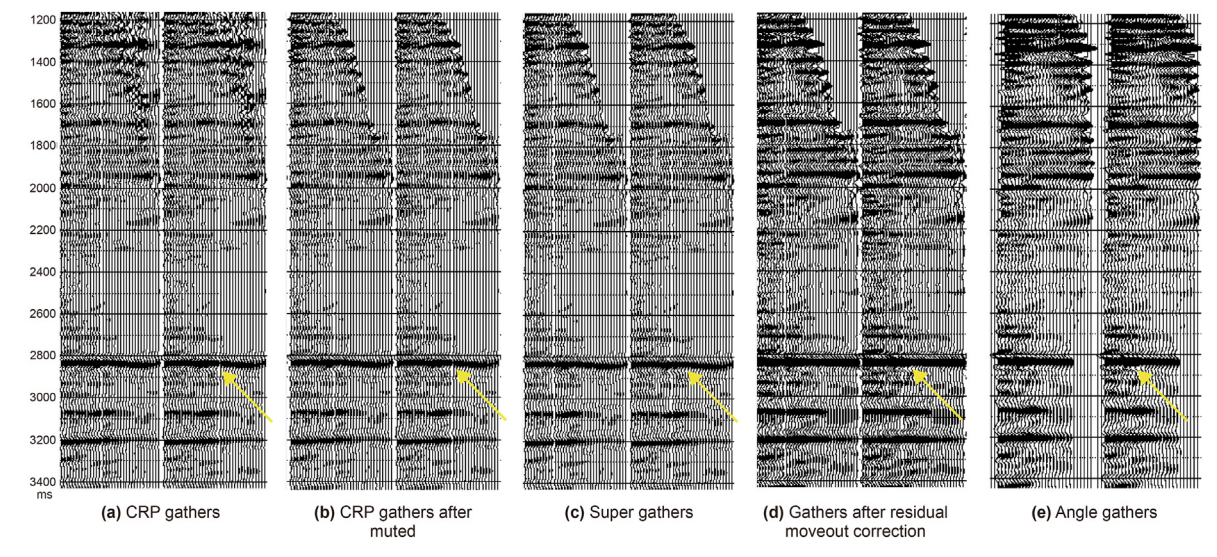
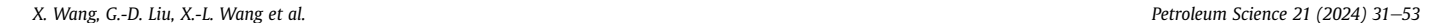


Fig. 7. Pre-stack gather conditioning processes. (a) CRP gathers, (b) CRP gathers after muted, (c) super gathers, (d) gathers after residual moveout correction, (e) angle gathers.



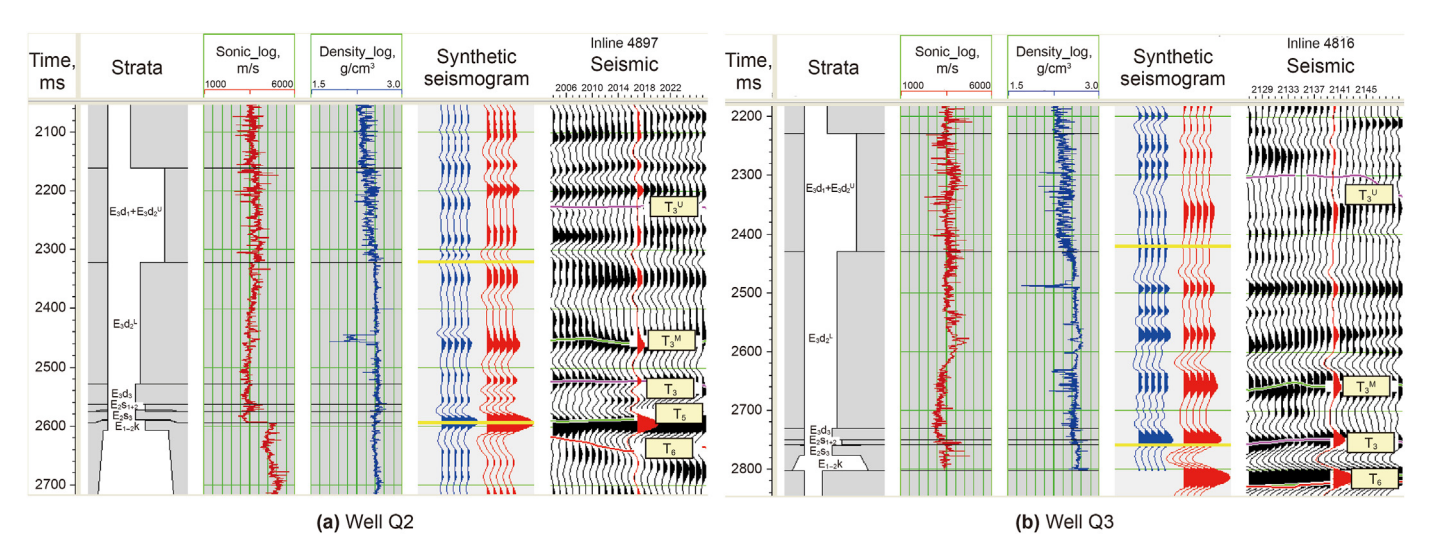


Fig. 8. Synthetic seismogram results of Well Q2 and Q3. (a) Well Q2, (b) Well Q3.

black curves on the left are the TOC and S_2 curves predicted by BP neural network method, and the red curves are the TOC and S_2 curves after time shift, smoothing and filtering) (Figs. 10 and 11).

The multiple attributes of the seismic traces near wells are extracted to combine the values of P-wave impedance, P-wave velocity, and density inversion results for multi-attributes analysis. Tables 1 and 2 are the TOC and S₂ multi-attributes correlations analysis results, respectively. It can be seen that when performing TOC multi-attributes analysis prediction. It is found that when the number of attributes is 5 (reciprocal of P-wave velocity, reciprocal of density, integrated absolute amplitude, dominant frequency, and reciprocal of P-wave impedance) (Table 1), the correlation coefficient is the highest and the error is the lowest. The correlation coefficient between the logging prediction TOC curves and seismic near wells prediction TOC for 13 wells is 0.6378, and the overall correlation coefficient is 0.7797 when using neural network training. When performing S₂ multi-attributes analysis prediction, the highest correlation coefficient and the lowest error were found when the number of attributes was 3 (reciprocal of P-wave velocity, reciprocal of P-wave impedance, and integrated absolute amplitude) (Table 2), the overall correlation coefficient between the logging predicted S₂ curves and the seismic near wells prediction S₂ for 13 wells is 0.6187, and the overall correlation coefficient is 0.7175 when using neural network training.

4. Results

4.1. OM abundance of source rocks

OM abundance evaluation is an important part of source rocks research (Peters, 1986; Hakimi and Ahmed, 2016). TOC, S_1 , S_2 , and genetic potential ($S_1 + S_2$) are used to evaluate the OM abundance of source rocks in the southwestern Bozhong Sag. Table 3 shows the OM abundance characteristic parameters of source rocks in southwestern Bozhong Sag. There are many sedimentary facies types in this area, including semi-deep and deep lake facies, braided river delta, sublacustrine fan, shore and shallow lake facies. The debris samples may be silty mudstone or siltstone, resulting in low TOC and T_{max} values.

The TOC of $E_3d_2^1$ source rocks ranges from 0.35% to 3.56% (avg. 0.85%), S_2 values are 0.18 to 15.57 mg/g (avg. 2.30 mg/g). The TOC of E_3d_3 source rocks ranges from 0.45% to 5.33% (avg. 2.19%); S_2 values are 0.13 to 31.03 mg/g (avg. 8.03 mg/g). The TOC of E_2S_{1+2} source rocks ranges from 0.25% to 6.90% (avg. 2.84%); S_2 ranges from 0.24

to 54.29 mg/g (avg. 12.93 mg/g). The TOC of E_2s_3 source rocks ranges from 0.80% to 7.76% (avg. 3.10%); S_2 mainly ranges from 1.27 to 58.32 mg/g (avg. 14.75 mg/g) (Table 3).

Based on the cross-plots between the S_2 and TOC (Fig. 12a), the cross-plots between the S_1+S_2 and TOC (Fig. 12b), the frequency distribution of TOC and S_1+S_2 (Fig. 12c and d), it can be seen that the OM abundance of Shahejie Formation is higher than that of Dongying Formation. E_2s_{1+2} and E_2s_3 source rocks have higher OM abundance values, which indicating better hydrocarbon generative potential. The hydrocarbon generation potential of E_3d_3 is relatively weak, which are evaluated as fair-good source rocks. The $E_3d_2^{\rm L}$ source rocks are poor to fair quality source rocks, the hydrocarbon generation potential of $E_3d_2^{\rm L}$ is relatively poor (Fig. 12).

4.2. Logging prediction results and comparison

Comparing the determination coefficient R^2 and the average relative error of four methods (Fig. 13 and Table 4). The generalized $\Delta \log R$ method has a higher prediction accuracy compared with Passy's method because it takes into account intensive compaction of source rocks in terrestrial facies; the correlation coefficient R^2 and average relative error of the generalized $\Delta \log R$ method are slightly better than multiple linear regression method. Compared with the other three methods, the prediction accuracy of BP neural network method is higher (Fig. 13).

According to the comparison results of correlation coefficients of each TOC prediction method (Table 4), it can also be seen that the generalized $\Delta log R$ method has better results for different sedimentary facies prediction models than the Passy's $\Delta log R$ method. For example, the determination coefficients are significantly improved in the semi-deep and deep lacustrine facies of $E_3d_2^L$ and E₃d₃ source rocks, while the correlation coefficients of the generalized $\Delta log R$ and the multiple linear regression methods have their own advantages, respectively. It is difficult to compare and prioritize the four models of different sedimentary facies, so it is necessary to conduct a unified analysis; the determination coefficient R^2 of BP neural network method is roughly above 0.80 in different sedimentary facies models, which is higher than the other three methods. The prediction accuracy of BP neural network is better than multiple linear regression and $\Delta logR$ series methods in southwestern Bozhong Sag.

According to the above analysis, the S_2 of source rocks in southwestern Bozhong Sag was also predicted using BP neural network method. Fig. 14 shows the TOC and S_2 prediction profiles of

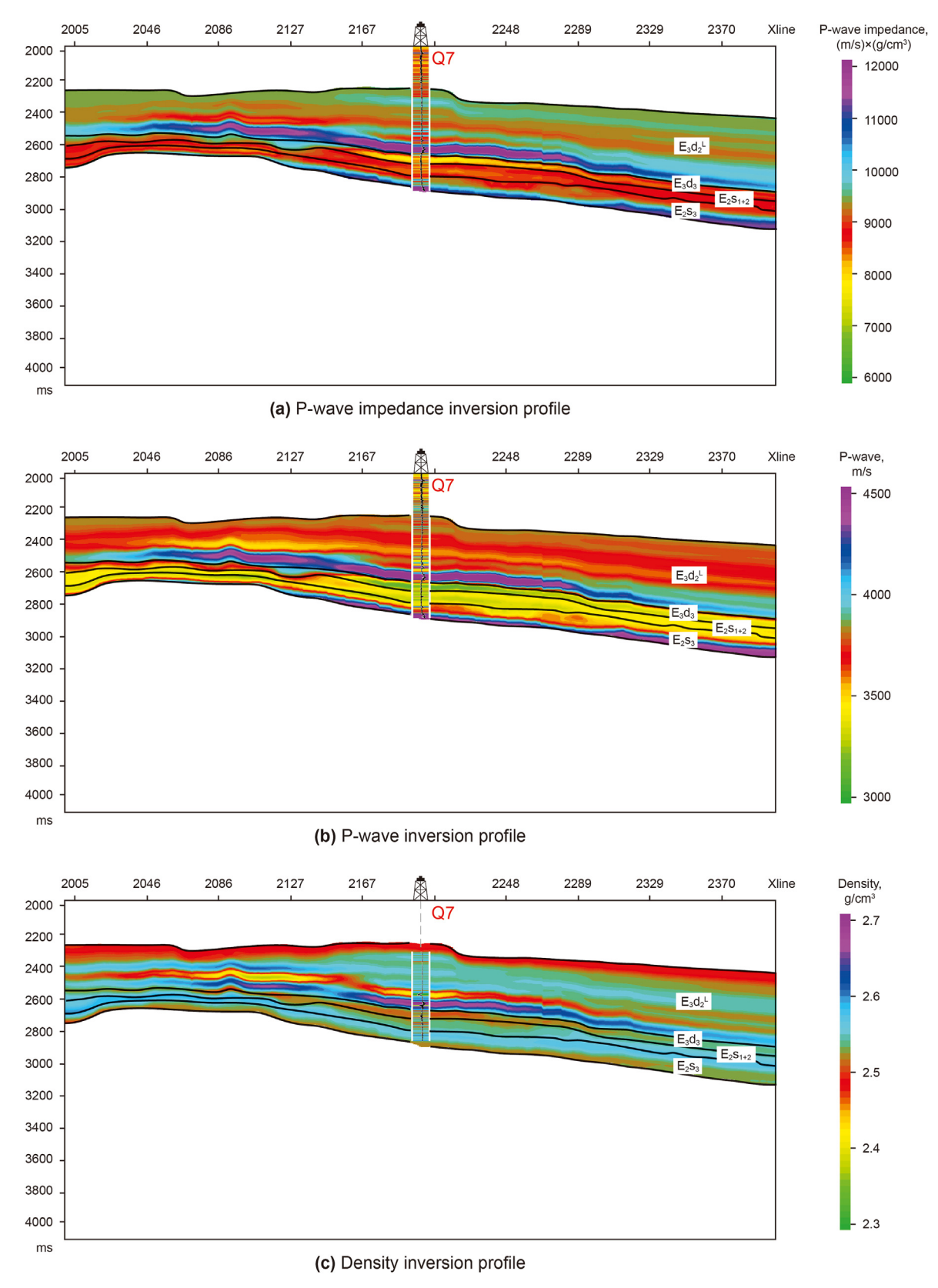


Fig. 9. Pre-stack simultaneous inversion results. (a) P-wave impedance, (b) P-wave, (c) Density.

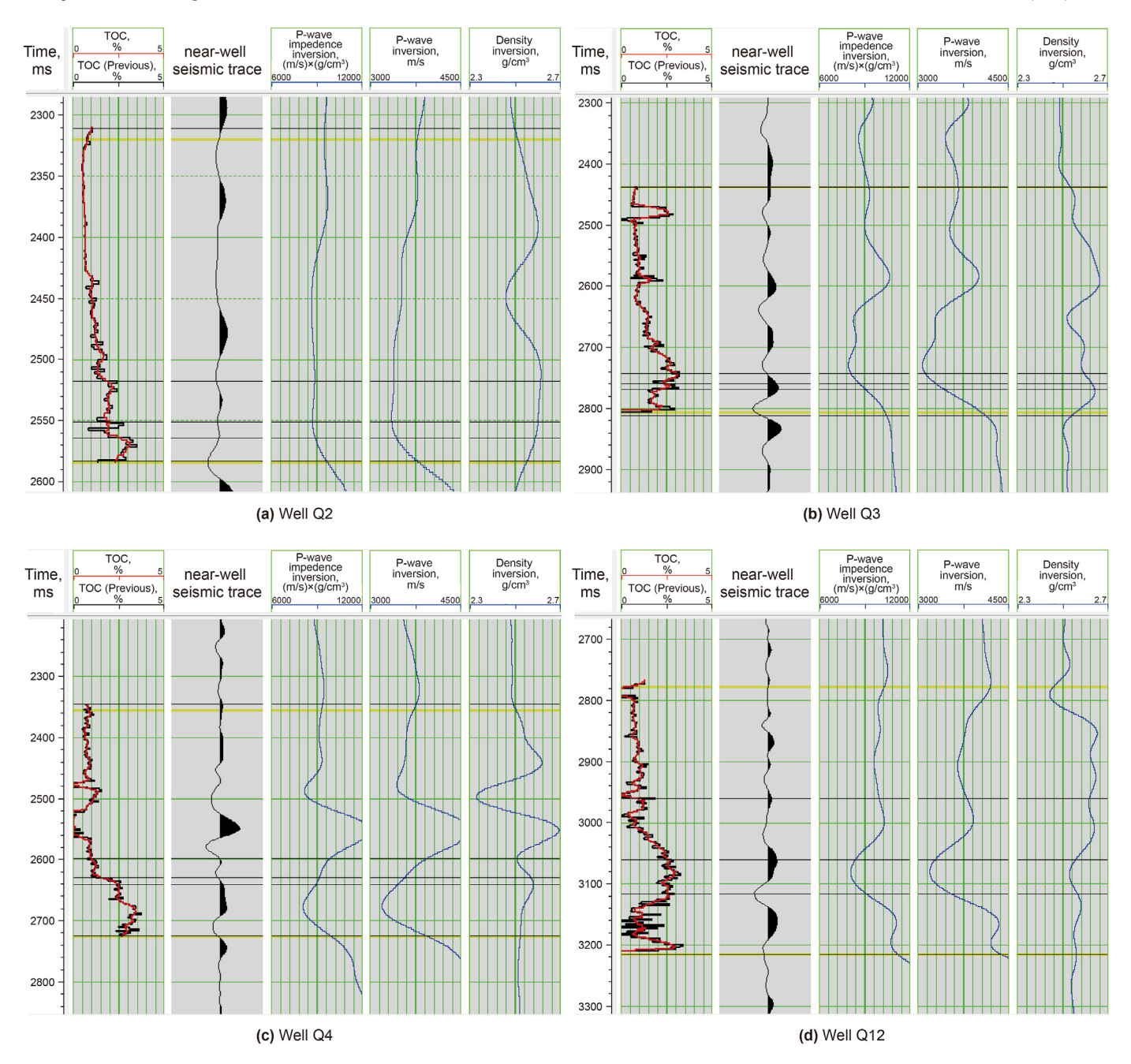


Fig. 10. Calibration diagram of TOC curves of typical wells and inversion trace of seismic data, P-wave impedance, P-wave velocity and density inversion results near wells. (a) Well Q2, (b) Well Q3, (c) Well Q4, (d) Well Q12.

well Q3 in the study area, and it can be obviously seen that the prediction results of BP neural network method in TOC and S_2 are in good agreement with the organic geochemical data. The OM abundance (TOC, S_2) values of $E_3d_2^L$ source rocks are low, the OM abundance values of the source rocks of E_2s_{1+2} and E_2s_3 are higher, and that in E_3d_3 source rocks are medium (Fig. 14).

4.3. Seismic prediction results of organic matter abundance

Figs. 15 and 16 show the TOC and S_2 seismic prediction profiles across the inversion wells, and the logging prediction TOC and S_2 curves are inserted at the well locations. The logging and seismic near well prediction results correlation coefficient for TOC is 0.7797, and the logging and seismic near well prediction results correlation

coefficient for S_2 is 0.7175, indicating that the neural network combined with seismic multi-attributes (post-stack seismic attributes, P-wave velocity, P-wave impedance and density inversion results) to predict TOC and S_2 of source rocks is feasible (Figs. 15 and 16).

In order to prove the prediction accuracy of the model, we used well Y3 that was not involved in pre-stack simultaneous inversion, to test the model (Fig. 17), and obtained the TOC and S_2 profiles across the well Y3. The logging and seismic near well prediction results correlation coefficient for TOC is 80.32%, and the average relative error is 10.58%. However, the S_2 value of the seismic near well Y3 (especially the source rocks of E_3d_3 interval) is high (the value ranges from 5.2 to 8.5), which is consistent with the trend of prediction results of logging method, indicating that the prediction

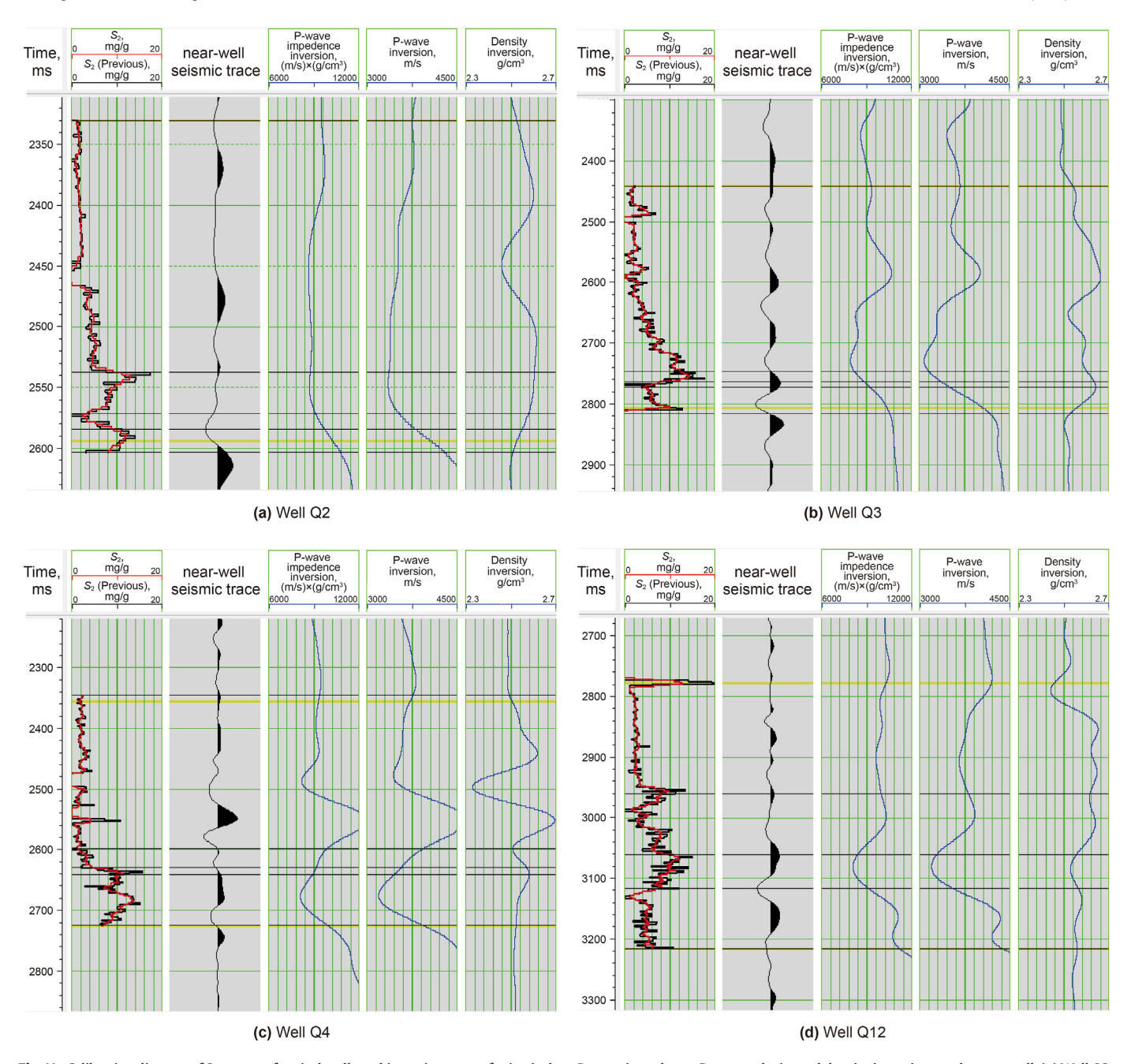


Fig. 11. Calibration diagram of S₂ curves of typical wells and inversion trace of seismic data, P-wave impedance, P-wave velocity and density inversion results near well. (a) Well Q2, (b) Well Q3, (c) Well Q4, (d) Well Q12.

Table 1Table of TOC and seismic multi-attributes correlation analysis.

| Target curve | Final attribute | Training error | Validation error | |
|--------------|-----------------------------------|----------------|------------------|--|
| TOC | Reciprocal of P-wave velocity | 0.775878 | 0.806666 | |
| TOC | Reciprocal of density | 0.752918 | 0.787887 | |
| TOC | Integrated absolute amplitude | 0.736557 | 0.790879 | |
| TOC | Dominant frequency | 0.721891 | 0.794449 | |
| TOC | Reciprocal of P-wave impedance | 0.708371 | 0.767903 | |
| TOC | Average frequency | 0.692053 | 0.779249 | |
| TOC | Amplitude weighted phase | 0.688232 | 0.778316 | |
| TOC | Instantaneous phase | 0.685239 | 0.777785 | |
| TOC | Apparent polarity | 0.683159 | 0.783618 | |
| TOC | Derivative of instantaneous phase | 0.682065 | 0.786299 | |
| TOC | Amplitude weighted cosine phase | 0.679798 | 0.785816 | |

Table 2Table of S₂ and seismic multi-attributes correlation analysis.

| Target curve | Final attribute | Training error | Validation error | |
|----------------|--------------------------------|----------------|------------------|--|
| S ₂ | Reciprocal of P-wave velocity | 3.104438 | 3.286747 | |
| S_2 | Reciprocal of P-wave impedance | 2.828075 | 2.991783 | |
| S_2 | Integrated absolute amplitude | 2.748946 | 2.949182 | |
| S_2 | Density squared | 2.719773 | 3.392887 | |
| S_2 | Amplitude weighted frequency | 2.692451 | 3.379546 | |
| S_2 | Dominant frequency | 2.661405 | 3.444809 | |
| S_2 | Amplitude weighted phase | 2.640017 | 3.439983 | |
| S_2 | Average frequency | 2.627350 | 3.570451 | |
| S_2 | Apparent polarity | 2.618618 | 3.626040 | |
| S_2 | Amplitude envelope | 2.612385 | 3.633032 | |
| S_2 | Instantaneous phase | 2.606557 | 3.631869 | |

Table 3Geochemical characteristics of the source rocks.

| Formation | TOC, % | S ₁ , mg/g | S ₂ , mg/g | S ₁ +S ₂ , mg/g | T _{max} , °C | HI, mg/g |
|--------------|------------------|-----------------------|-----------------------|---------------------------------------|-----------------------|------------------------|
| $E_3d_2^L$ | 0.35-3.56 (0.85) | 0.01-5.26 (0.47) | 0.18-15.57 (2.30) | 0.28-16.25 (2.78) | 402-451 (437) | 49.12-630.44 (242.21) |
| E_3d_3 | 0.45-5.33 (2.19) | 0.03-6.38 (1.91) | 0.13-31.03 (8.03) | 0.33-32.16 (9.93) | 393-493 (441) | 8.96-774.48 (334.45) |
| E_2s_{1+2} | 0.25-6.90 (2.84) | 0.02-6.21 (2.20) | 0.24-54.29 (12.93) | 0.26-59.80 (15.11) | 397-457 (434) | 14.59-1019.53 (393.45) |
| E_2s_3 | 0.80-7.76 (3.10) | 0.16-7.59 (2.16) | 1.27-58.32 (14.75) | 1.62-63.99 (16.93) | 418-468 (439) | 52.27-1269.75 (426.85) |

Note: The values in the brackets represent the arithmetic mean.

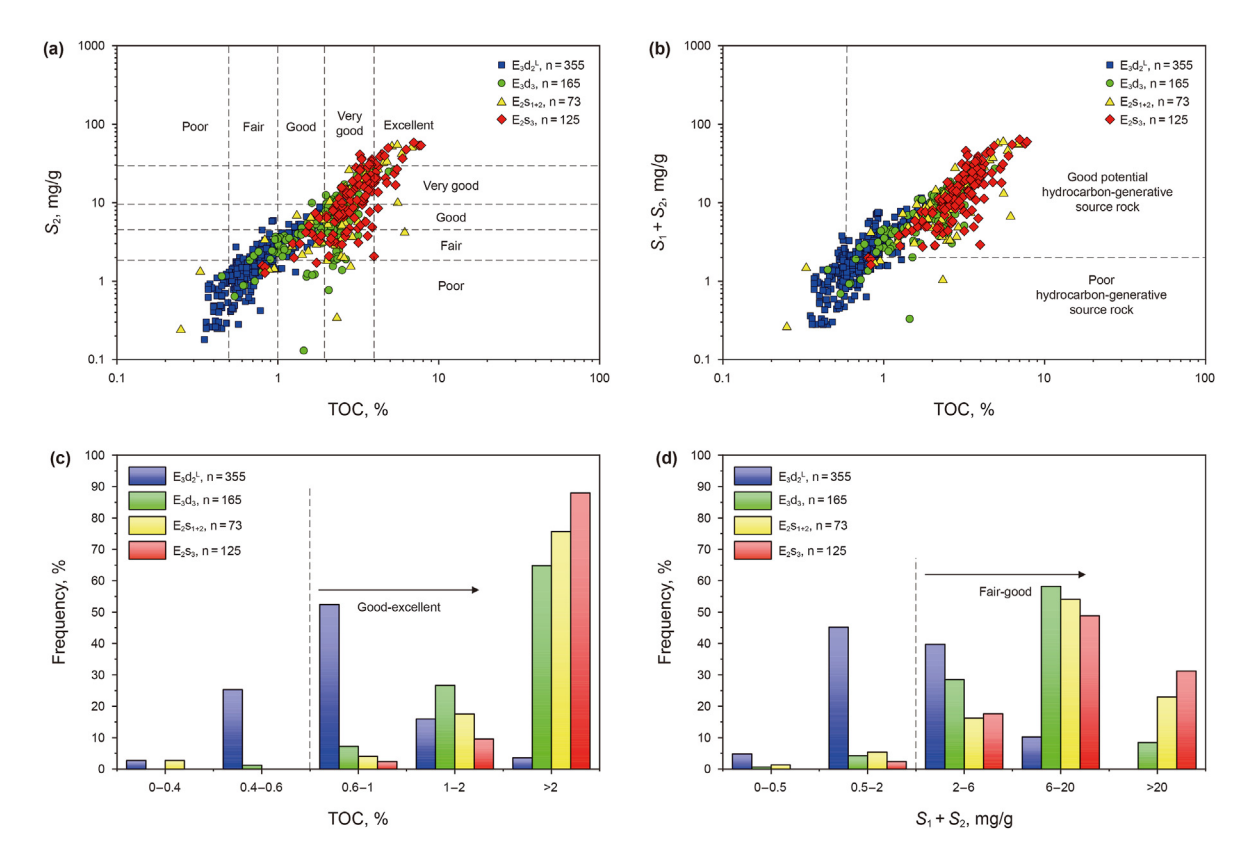


Fig. 12. Geochemical characteristics of source rocks in the study area. (a) Plot of TOC vs. S₂ (after Hakimi and Ahmed, 2016), (b) TOC vs. S₁+S₂ (after Hakimi and Ahmed, 2016), (c) Frequency diagrams of TOC, (d) Frequency diagrams of S₁+S₂.

model has better prediction ability, and that the area near well Y3 is the high-quality source rocks deposition area with good hydrocarbon generation potential (Fig. 17).

The advantage of seismic method is that it has a high horizontal resolution, and can effectively identify the source rocks that have no samples. Therefore, the evaluation of TOC and S_2 requires not only comparing the seismic near well prediction results with the

logging prediction results, but also making plane distribution of the TOC and S₂ seismic prediction results, and further using the sedimentary facies maps to verify the credibility of this method (Figs. 18, 19 and 20).

As in Fig. 18a, the black dotted bordered rectangle is the seismic workings. During the $E_3d^L_2$ depositional stage, there are mainly braided river delta facies within the seismic workings (the areas of

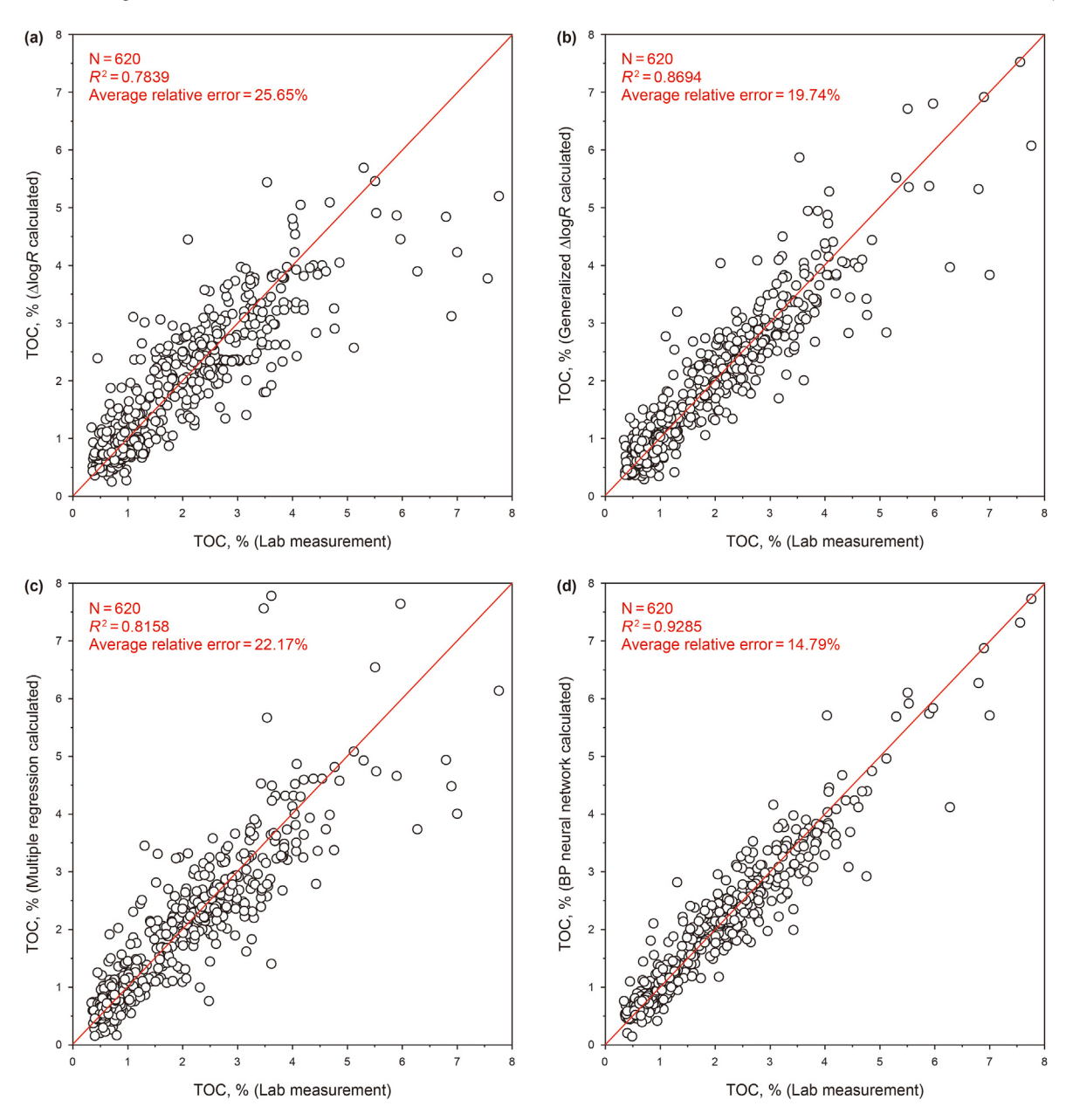


Fig. 13. Four methods to predict TOC determination coefficients, average relative errors analysis charts. (a) Passey's $\Delta logR$ method, (b) generalized $\Delta logR$ method, (c) multiple linear regression method, (d) BP neural network method.

Table 4 Comparison of determination coefficient \mathbb{R}^2 of different TOC prediction methods.

| Strata | Sedimentary facies | $\Delta log R$ method | Generalized $\Delta log R$ method | Multiple linear regression | BP neural network |
|-------------------------------|--|-----------------------|-----------------------------------|----------------------------|-------------------|
| $E_3d_2^L$ | Braided river delta | 0.7632 | 0.7822 | 0.7505 | 0.9086 |
| | Fan dalta | 0.0482 | 0.6187 | 0.7056 | 0.8492 |
| | Shore-shallow lacustrine | 0.6889 | 0.8125 | 0.3590 | 0.8305 |
| | Semi-deep and deep lacustrine | 0.1371 | 0.6131 | 0.6317 | 0.8026 |
| | Sublacustrine fan | 0.1707 | 0.2096 | 0.3409 | 0.8131 |
| E ₃ d ₃ | Braided river delta and fan dalta | 0.6911 | 0.8735 | 0.8656 | 0.9520 |
| | Shore-shallow lacustrine | 0.4012 | 0.8512 | 0.7653 | 0.8755 |
| | Semi-deep and deep lacustrine | 0.0195 | 0.5633 | 0.6216 | 0.7162 |
| | Sublacustrine fan | 0.5473 | 0.5518 | 0.5256 | 0.9088 |
| E_2s_{1+2} | Shore-shallow lacustrine and braided river delta | 0.5124 | 0.6912 | 0.4290 | 0.8156 |
| E ₂ s ₃ | Braided river delta | 0.5583 | 0.6932 | 0.7009 | 0.9254 |
| | Fan dalta | 0.1972 | 0.5281 | 0.4990 | 0.6429 |
| | Semi-deep and deep lacustrine | 0.2960 | 0.4676 | 0.3640 | 0.6851 |

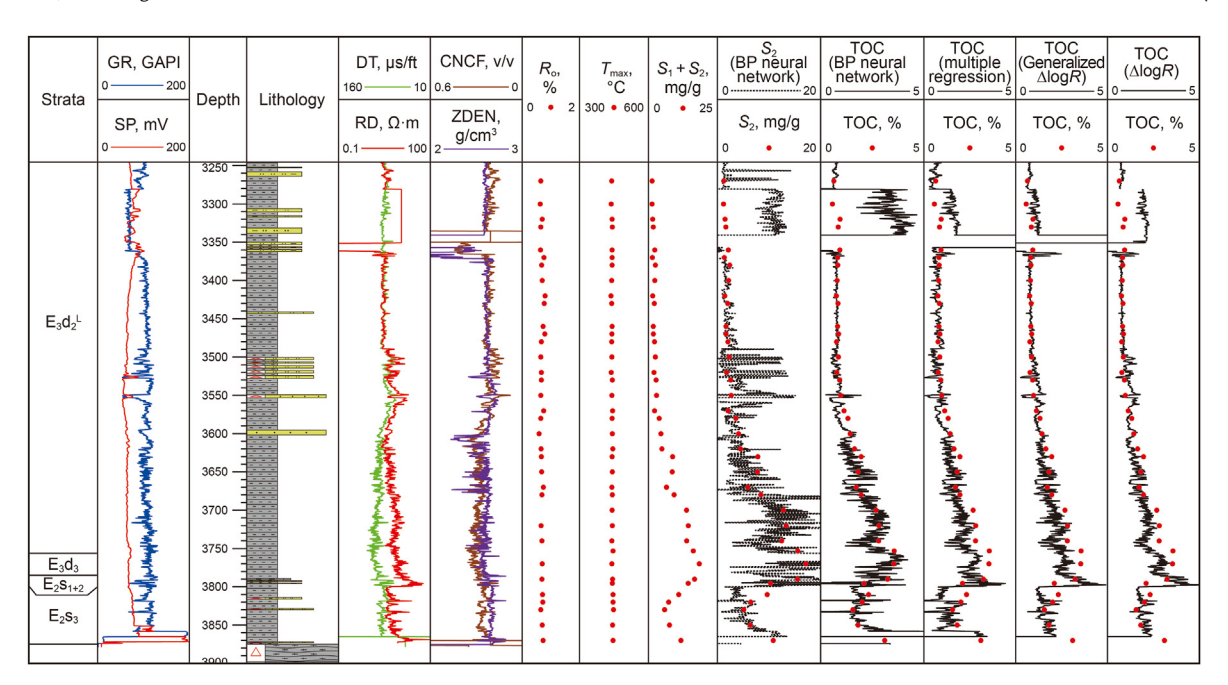
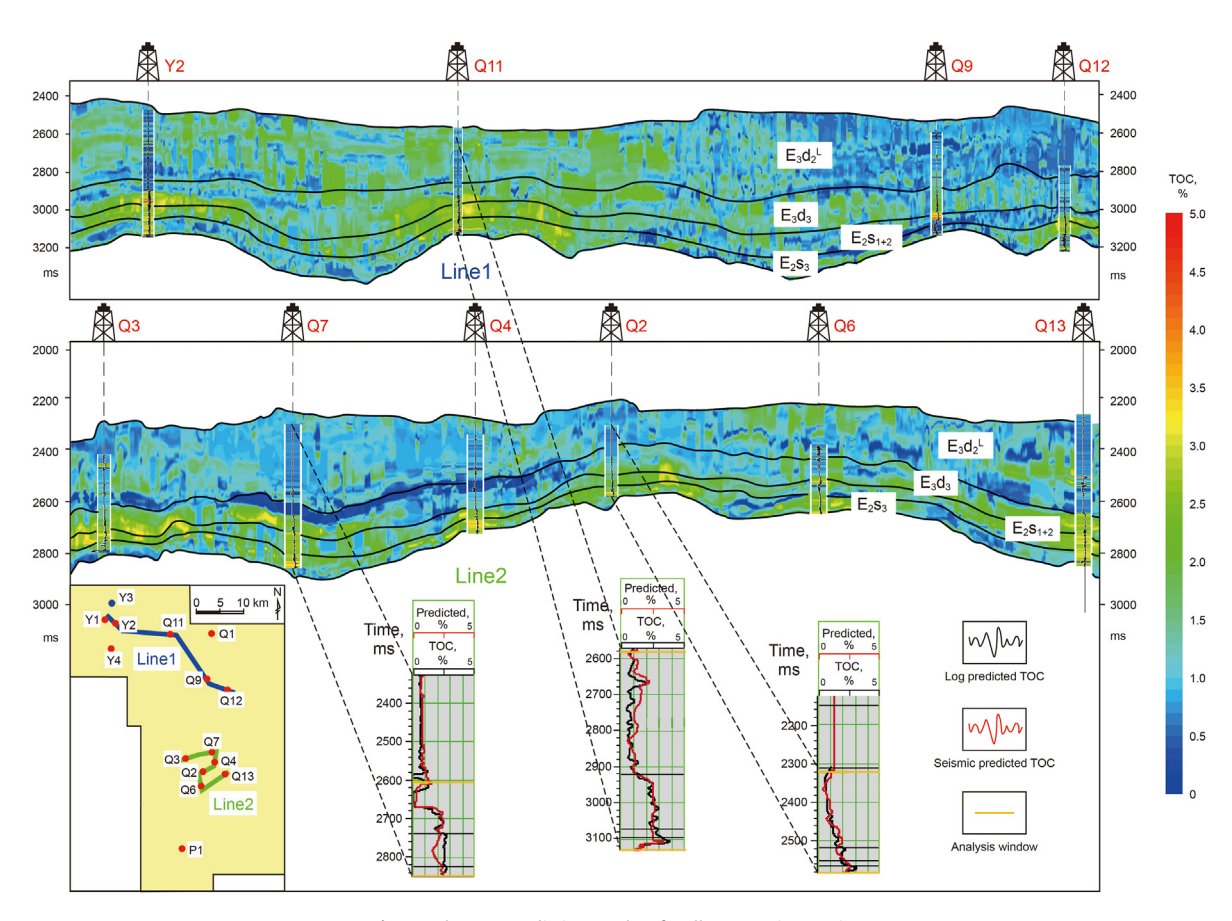


Fig. 14. TOC and S₂ prediction results of well Q3.



 $\textbf{Fig. 15.} \ \ \textbf{The TOC prediction results of wells connection section.}$

well Q2, Q3, Q4, Q6, Q7 and Q13), which are not conducive to the formation of good-quality source rocks, while the areas of well Y1, Y2, Q1 and Q11 are sublacustrine fan, semi-deep and deep lacustrine facies, which are conducive to the deposition of good-quality

source rocks. As in Figs. 19a and 20a, the TOC in the areas of well Y1, Y2, Q1 and Q11 ranges from 1.0% to 2.0% and S2 ranges from 2 to 6 mg/g, which are fair to good source rocks. The TOC in areas of well Q2, Q3, Q4, Q6, Q7 and Q13 ranges from 0% to 0.4% and S2 ranges

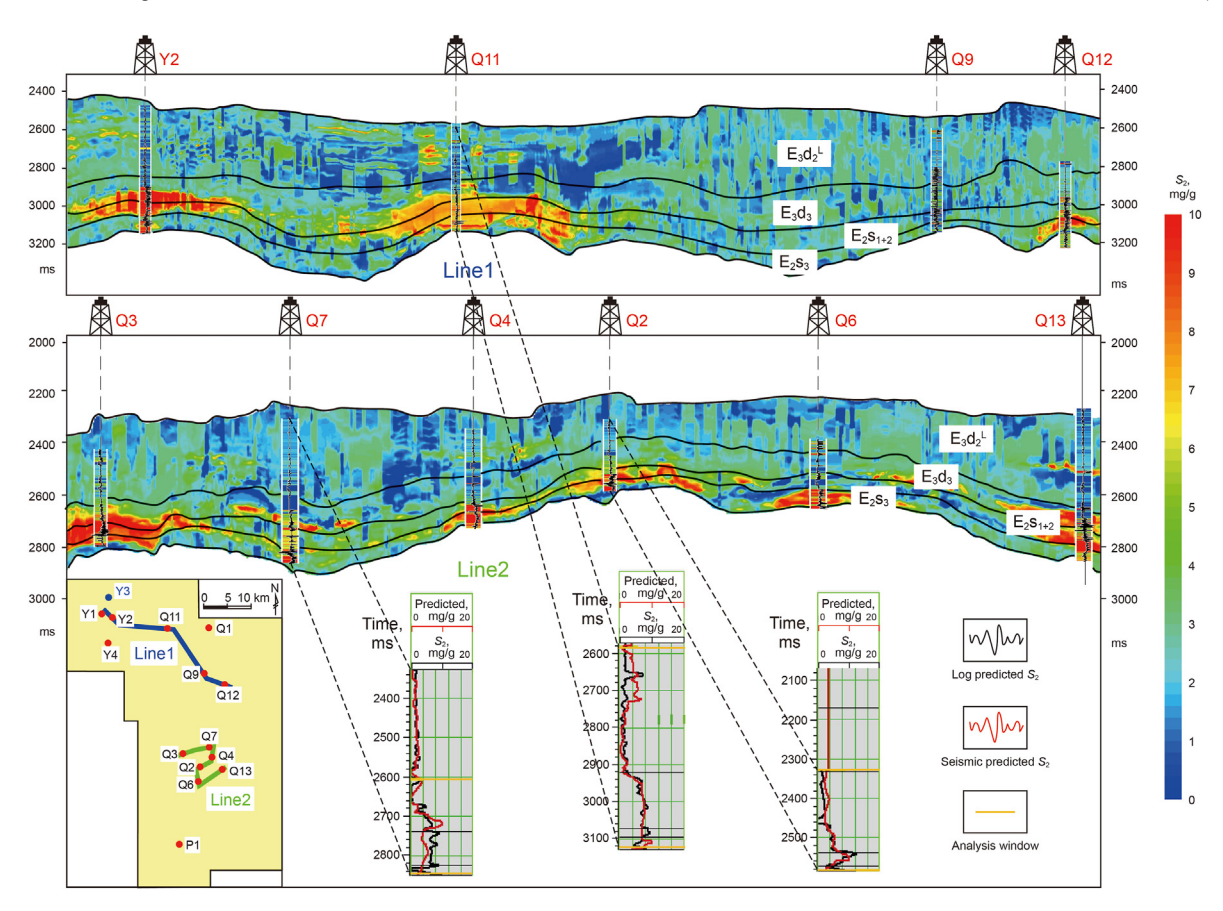


Fig. 16. The S₂ prediction results of wells connection section.

from 0 to 2 mg/g, and the quality of source rocks is poor. The OM abundance of source rocks in the north is better than that in the south, and shows a trend of gradually decreasing from north to south.

As in Fig. 18b, during the E_3d_3 depositional stage, the areas of well Y1, Y2, Y4, Q1 and Q11 in the seismic workings are mainly semi-deep and deep lacustrine facies, the areas of well Q2, Q3, Q4, Q6, Q7, Q13 and P1 are shore-shallow lacustrine facies, and the northern part is favorable for the deposition of good-quality source rocks. As Figs. 19b and 20b, the TOC in the areas of well Y4 and Q11 and the western part of the workings ranges from 1.0% to 2.5% and S2 ranges from 2 to 6 mg/g, which are fair to good quality source rocks, and TOC in the areas of well Q2, Q3, Q4, Q6, Q7 and Q13 ranges from 0.2% to 0.6% and S2 ranges from 1 to 3 mg/g, the source rocks are poor to fair quality.

As in Fig. 18c, during $E_{2}s_{1+2}$ depositional stage, the seismic workings are mainly shore-shallow lacustrine facies, and the western part of the workings are semi-deep and deep lacustrine facies. As in Figs. 19c and 20c, the TOC in areas of well Y2, Q3, Q7 and Q11 ranges from 1.0% to 3.0%, and S_2 ranges from 2 to 8 mg/g, which are good to very good quality source rocks, TOC in the areas of well Q1, Q9 and Q12 is low, ranging from 0.2% to 0.6%, and S_2 ranges from 1 to 4 mg/g, represent fair quality source rocks.

As in Fig. 18d, during the E₂s₃ depositional stage, semi-deep and deep lacustrine facies are developed in the areas of well Y1, Y2, Y4, Q4, Q7, Q9, Q11, Q12 and Q13, sublacustrine fan facies are developed in the areas of well Q2, Q3 and Q6, and shore-shallow lacustrine facies are developed in area of well Q1. As in Figs. 19d and 20d, the TOC in the areas of well Q2, Q3, Q4, Q6, Q7 and Q13 ranges from 1.0% to 3.0%, and S₂ ranges from 2 to 10 mg/g, which are very good

to excellent quality source rocks, and TOC in the areas of well Y1, Y4, Q1, and Q9 is lower, ranging from 0.6% to 1.0%, and S_2 ranges from 2 to 4 mg/g, source rocks are fair quality.

5. Discussions

5.1. Passey et al. (1990) method

Among the methods for estimating TOC from well logs, Passey's $\Delta log R$ method is based on rigorous petrophysical model derivation and includes fewer well logs (redundant information), using the Wyllie formula and the Archie formula to overlap the porosity logs (usually DT) with the resistivity logs (usually RD). The combination of sonic transit time logs and resistivity logs could eliminate the influence of porosity on the logging response from OM (Passey et al., 1990). However, this method requires the determination of the baseline value, and different baselines are used for different wells and even different intervals, which makes the operation of this method more complicated (Liu et al., 2014, 2021; Zhao et al., 2016). Furthermore, the determination of ΔTOC is mainly based on the empirical, geological settings and geochemical data, which also has significant uncertainty. The overlay-coefficient not only eliminates the effect of on the porosity logging response for OM, but also affects the relative ability to identify kerogen and hydrocarbon fluids. To determine the overlay-coefficient, the proportion of kerogen and hydrocarbon fluids in the source rock should be considered, and the overlay-coefficient value of 2 is not objective enough. Finally, LOM is introduced into the equation, which is generally obtained from a large number of sample analyses (such as vitrinite reflectance, thermal alteration index, Rock-Eval T_{max}

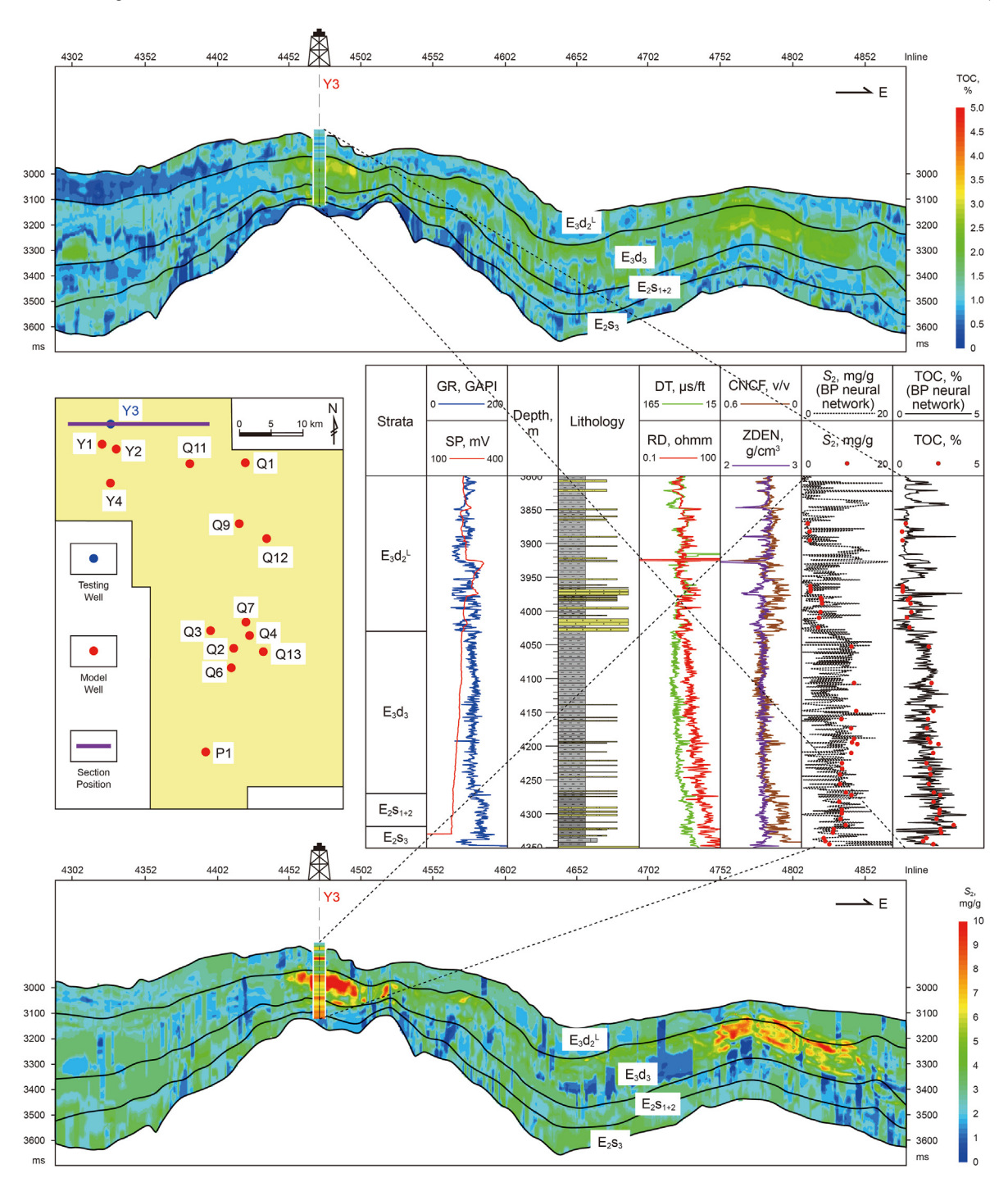


Fig. 17. The TOC and S_2 prediction results of the section cross the well Y3.

analysis), or from burial history and thermal history evaluation (Liu et al., 2014, 2021; Wang et al., 2016; Zhao et al., 2016; Zhu et al., 2019).

5.2. The generalized $\Delta logR$ method

The generalized $\Delta log R$ method includes GR and DEN logs, which take into account: A single log curve is easy to be interfered, and multiple logging curves have significant anti-interference ability. The radioactive elements such as U, Th and K usually contained in continental mudstone will lead to high natural gamma value. In

addition, terrestrial facies intervals have intensive compaction effect, while GR log is less affected by compaction effect by compaction and more sensitive to the changes of deep continental source rocks (Hu et al., 2015; Liu et al., 2021). The Δ logR method and its improvement methods are widely used in major petroliferous basins, including Songliao Basin, Bohai Bay Basin, Sichuan Basin (Liu et al., 2014, 2021; Hu et al., 2015; Zhao et al., 2016; Zhu et al., 2019) and the Western Basin of Canada (Wang et al., 2016). The Δ logR method and its improved methods have been applied effectively in both marine and terrestrial sequences. In particular, some large shale gas fields had been found in the Sichuan Basin in

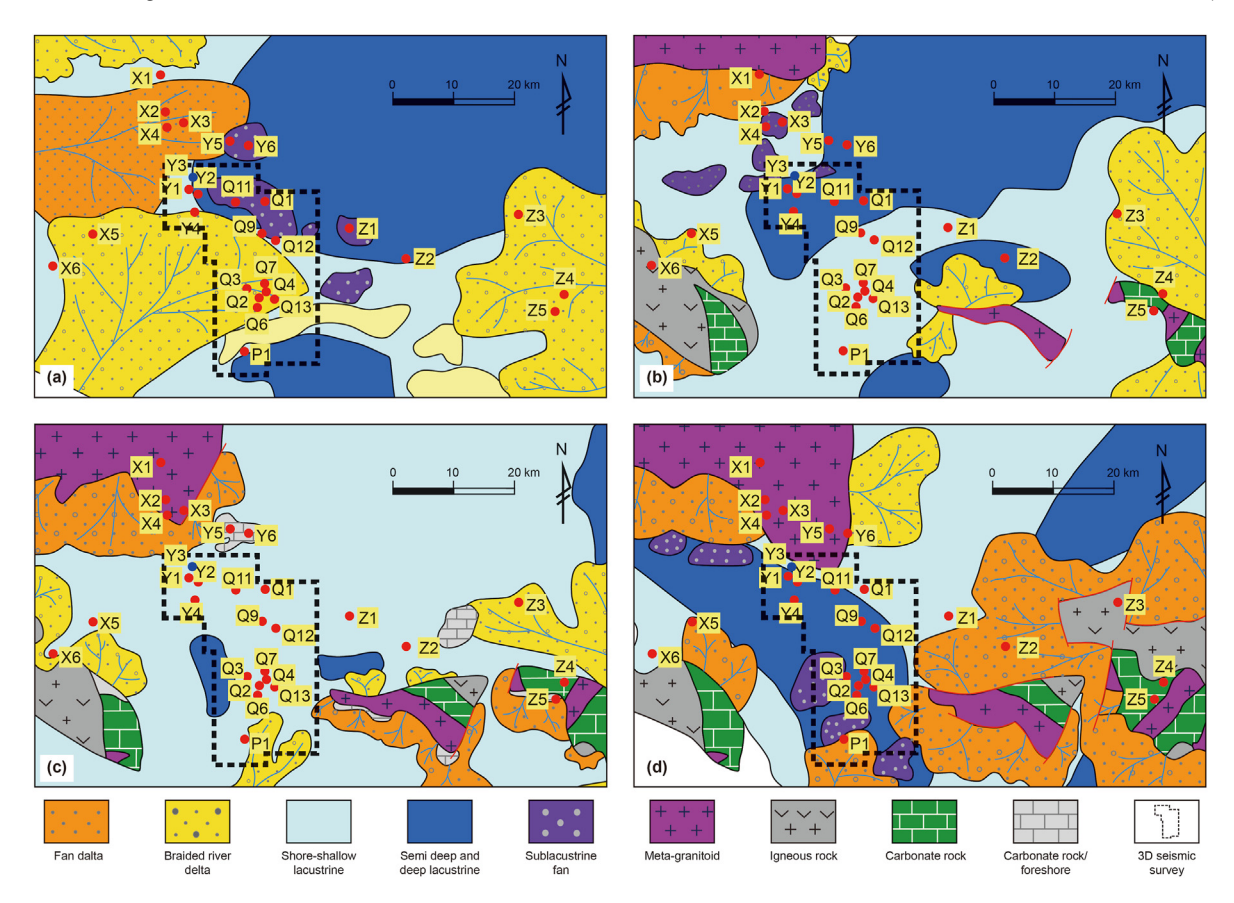


Fig. 18. Sedimentary facies diagrams of southwestern Bozhong Sag (modified from the Exploration and Development Research Institute of CNOOC Tianjin Branch). (a) E₃d^L₂, (b) E₃d₃, (c) E₂s₁₊₂, (d) E₂s₃.

recent years. The research on geophysical prediction of organic-rich mudstones has become focused issues (Zhao et al., 2016, 2020; Chen et al., 2018; Zhu et al., 2019). In this study, it is found that the prediction accuracy of the $\Delta log R$ method is relatively low, which may be related to the complexity of geological settings of the Bozhong Sag. The geological settings of rapid subsidence results in significant differences in the burial depth, sedimentary facies, lithology and organic geochemical characteristics of source rocks from each well.

5.3. Multiple regression method

Compared with $\Delta log R$ method, the multiple regression method is relatively simple to operate. In this study, the correlation coefficients of resistivity and TOC, S₂ are 0.5731 and 0.3425, respectively, which are lower than the sonic transit time and density, which may be related to the low maturity of source rocks in the southwestern Bozhong Sag. There are no hydrocarbon liquids displace formation water in the pores (Hao et al., 2010, 2011; Jiang et al., 2016; Wang et al., 2020). The comparison of prediction results shows that the prediction accuracy of multiple regression method is better than that of Passey's method. The generalized $\Delta \log R$ method uses DT, DEN, RD and GR logs, which are the same as those used by multiple linear regression, so the prediction accuracy of the multiple regression method and the generalized $\Delta log R$ method is similar. However, the limitations of multiple regression method should not be ignored. The formulas obtained by fitting are not universal enough, different formulas need to be fitted in different geological settings, different basins and even different intervals (Mendelzon and Toksoz, 1985; Aziz et al., 2020; Liu et al., 2021). The high correlation coefficients of DT and DEN logs with TOC and S_2 indicate that it is feasible to predict OM abundance in this region by using seismic pre-stack inversion (pre-stack P-wave velocity and density inversion results) combined with post-stack seismic attributes.

5.4. BP neural network method

The relationships between TOC and S2 and well logging are difficult to be expressed by dominant function, which belongs to nonlinear problem, because source rocks are a kind of sedimentary rocks with significant heterogeneity (Huang and Williamson, 1996), mineral composition, pore structure, fluid properties and kerogen affect the petrophysical properties of source rocks, which lead to the great differences in well logging values (Vernik and Nur, 1992; 1996; Carcione, 2000, 2001, 2011, 2015; Hansen et al., 2019), while the neural network methods have incomparable superiority in nonlinear calculation (Kamali and Mirshady, 2004; Bolandi et al., 2015). Neural network methods have been widely used in OM abundance prediction of source rocks (Huang and Williamson, 1996; Kamali and Mirshady, 2004; Bolandi et al., 2015; Tan et al., 2015; Verma et al., 2016; Ji et al., 2018; Wang et al., 2017; Shalaby et al., 2019; Wang et al., 2019; Zhao et al., 2021). Although BP neural network method is better than $\Delta log R$ methods in prediction accuracy, it does not establish the internal relationships between OM and rock physical parameters, and only builds the neural network model from the perspective of mathematics, without considering the influence of geological settings, and there may be overfitting situation (Liu et al., 2021). In this study, for BP neural network method, the correlation coefficient between the prediction values and the

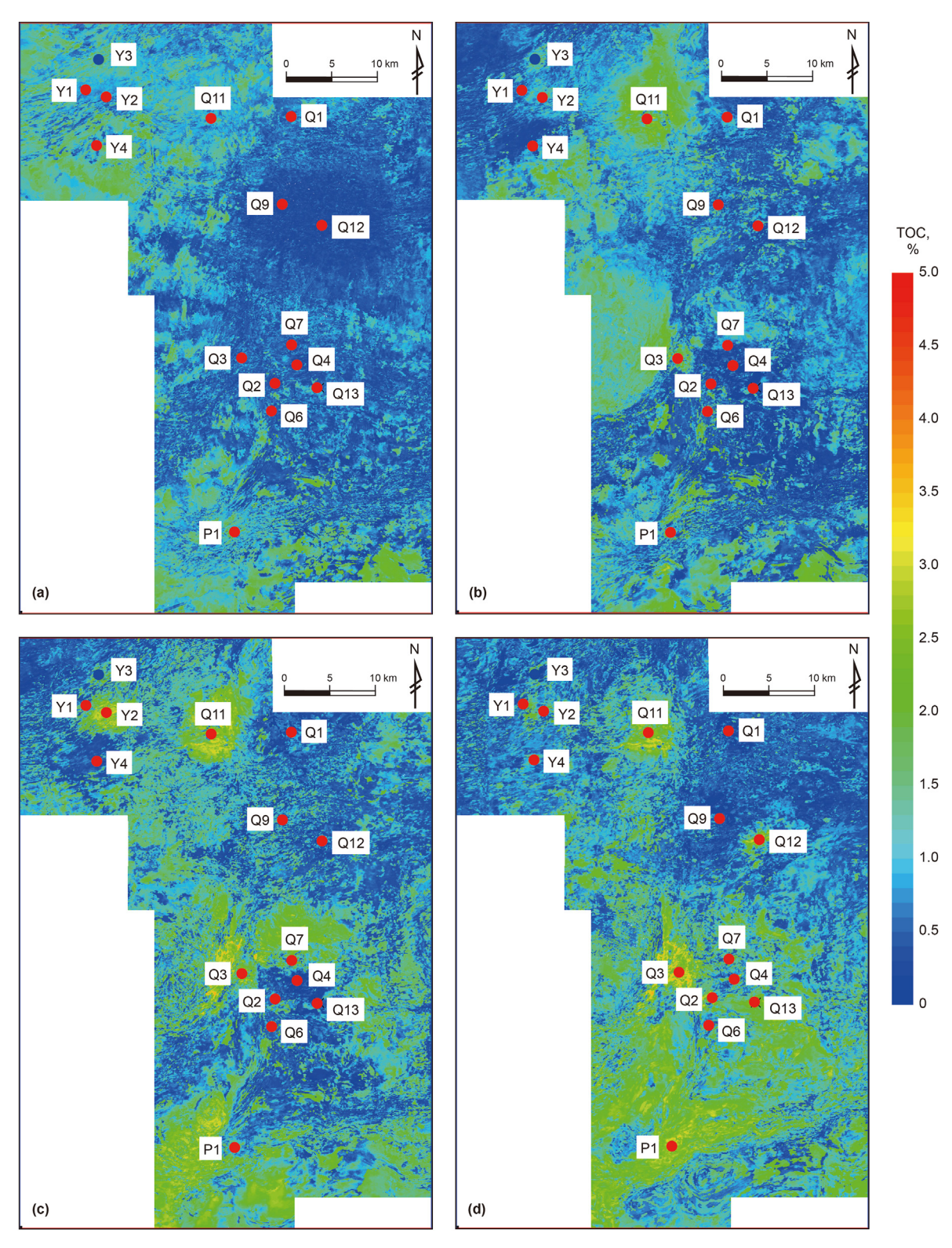


Fig. 19. The TOC planar distribution. (a) $E_3d_2^L$, (b) E_3d_3 , (c) E_2s_{1+2} , (d) E_2s_3 .

measured values of TOC is 0.9285, and the average relative error is 14.79%, indicating that its accuracy is better than the other three methods. The source rocks $(E_3d_2^{\rm l}, E_3d_3, E_2s_{1+2}, E_2s_3)$ of the southwestern Bozhong Sag are typical continental mudstones. The tectonic movement and sedimentary environment changes in Bozhong Sag resulted in the heterogeneity of source rocks and

differences in the OM enrichment models (Hao et al., 2011; Wang et al., 2020). Therefore, the various TOC prediction methods should be compared to select one that is more consistent with the geological settings of the study area.

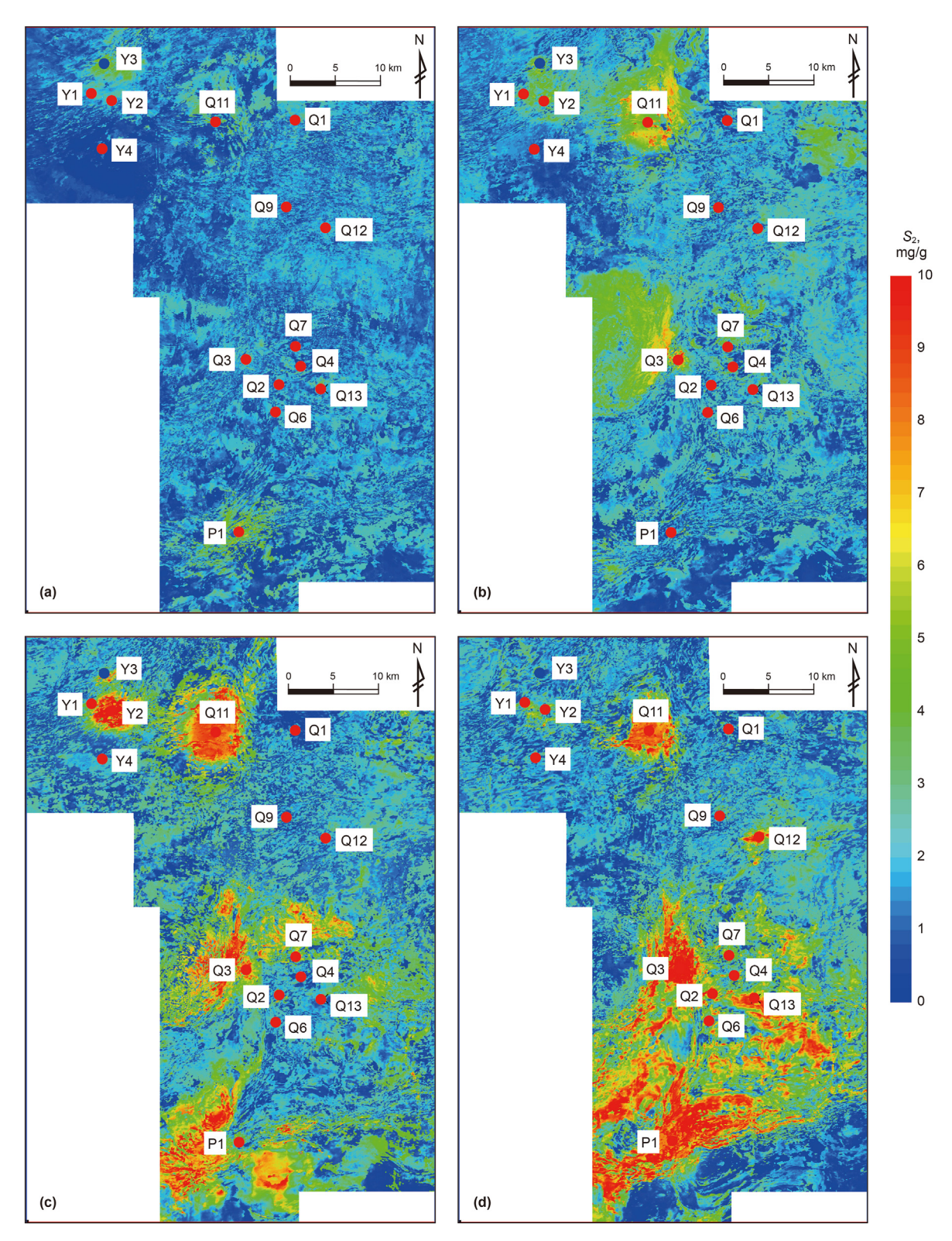


Fig. 20. The S_2 planar distribution. (a) $E_3d_2^L$, (b) E_3d_3 , (c) E_2s_{1+2} , (d) E_2s_3 .

5.5. Seismic multi-attributes fusion method

Among the methods for estimating TOC and S_2 from seismic, post-stack seismic data generally contain less information, and the logical relationships between the post-stack seismic attributes

(amplitude, frequency, phase, etc.) and the OM abundance are not clear enough. Only P-wave impedance inversion results could be obtained by post-stack seismic inversion. In the southwestern Bozhong Sag, it is found that the TOC and S_2 are positively correlated with DT (negatively correlated with P-wave velocity) and

negatively correlated with density through petrophysical correlation diagram (Fig. 5). Therefore, the P-wave impedance, P-wave velocity and density inversion results obtained by pre-stack simultaneous inversion could predict the OM abundance (TOC and S₂) more effectively, and contain more information from prestack seismic data, thus achieving higher inversion accuracy. However, compared with post-stack inversion, pre-stack inversion has a larger amount of computation and a longer operation time, so it is not widely used in the industry (Hampson et al., 2005; Sen and Stoffa, 2013; Chen et al., 2018). In this study, when predicting TOC of source rocks, we found that the five attributes reciprocal of P-wave velocity, reciprocal of density, integrated absolute amplitude, dominant frequency and reciprocal of P-wave impedance are the best and have the lowest prediction error. These five attributes include pre-stack inversion, post-stack inversion and post-stack seismic attributes. Moreover, TOC has the best correlation with the reciprocal of P-wave velocity and reciprocal of density, indicating that the method of combining pre-stack simultaneous inversion, post-stack inversion and post-stack seismic attributes is more effective in this study. The correlation coefficients of the seismic prediction results near well and logging prediction results are relatively high (TOC: 0.7797, S₂: 0.7175). Geochemical analysis of well Y3 also shows a high correlation between well logging and seismic predictions, and the plane prediction results are relatively consistent with the sedimentary facies map of the southwestern Bozhong Sag, it is an effective method for the research of source rocks in the areas with low-degree exploration.

6. Conclusions

Organic geochemical testing, petrophysical analysis, pre-stack and post-stack seismic inversion, and multi-attributes analysis are integrated to evaluate OM abundance of source rocks in southwestern Bozhong Sag, Bohai Bay Basin. A summary of key observations from this study follows:

- (1) The OM abundance of Shahejie Formation is higher than that of Dongying Formation in southwestern Bozhong Sag. E₂s₁₊₂ and E₂s₃ source rocks have the highest OM abundance, which indicating good to excellent hydrocarbon generative potential; E₃d₃ source rocks are fair to good quality source rocks; E₃d₂ source rocks have poor to fair hydrocarbon generative potential.
- (2) The accuracy of BP neural network method in predicting TOC and S_2 is higher than that of $\Delta logR$ series methods and multiple linear regression method.
- (3) The seismic near wells prediction results of TOC and S₂ correspond well with the logging prediction results, and the plane prediction results are highly consistent with the sedimentary facies. The multi-attributes method, which combines pre-stack seismic inversion, post-stack seismic inversion and seismic attributes, shows high horizontal resolution and compensates the limitations of geochemistry and well logging methods.

Declaration of competing interest

The authors declare that they have no known competing financial interests or personal relationships that could have appeared to influence the work reported in this paper.

Acknowledgements

We thank Tianjin Branch of China National Offshore Oil Company Ltd. for kindly providing source rock samples and part of the data in this study. We particularly wish to acknowledge the collaboration and enthusiastic support of Deying Wang and Xintao Zhang from the Tianjin Branch of CNOOC Ltd.

References

- Allen, M.B., Macdonald, D.I.M., Xun, Z., Vincent, S.J., Brouet-Menzies, C., 1997. Early Cenozoic two-phase extension and late Cenozoic thermal subsidence and inversion of the Bohai Basin, northern China. Mar. Petrol. Geol. 14 (7–8), 951–972. https://doi.org/10.1016/S0264-8172(97)00027-5.
- Aziz, H., Ehsan, M., Ali, A., Khan, H.K., Khan, A., 2020. Hydrocarbon source rock evaluation and quantification of organic richness from correlation of well logs and geochemical data: a case study from the sembar formation, Southern Indus Basin, Pakistan. J. Nat. Gas Sci. Eng. 81, 103433. https://doi.org/10.1016/ j.jngse.2020.103433.
- Badics, B., Avu, A., Mackie, S., 2015. Assessing source rock distribution in Heather and Draupne Formations of the Norwegian North Sea: a workflow using organic geochemical, petrophysical, and seismic character. Interpretation 3 (3), SV45–SV68. https://doi.org/10.1190/INT-2014-0242.1.
- Beers, R.F., 1945. Radioactivity and organic content of some Paleozoic shales. AAPG Bull. 29 (1), 1–22. https://doi.org/10.1306/10.1306/3D933700-16B1-11D7-8645000102C1865D.
- Bolandi, V., Kadkhodaie-Ilkhchi, A., Alizadeh, B., Tahmorasi, J., Farzi, R., 2015. Source rock characterization of the Albian Kazhdumi formation by integrating well logs and geochemical data in the Azadegan oilfield, Abadan plain, SW Iran. J. Petrol. Sci. Eng. 133, 167–176. https://doi.org/10.1016/j.petrol.2015.05.022.
- Cai, D.M., Zhao, D.J., Peng, J.S., Fu, L., Zeng, J.C., Cheng, Y.Q., 2018. High-quality hydrocarbon source rock identification and quantitative evaluation with multiattribute inversion: a case study of Liaodong south sub-sag, Bohai Basin. Oil Geophys. Prospect. 53 (2), 330–338. https://doi.org/10.13810/j.cnki.issn.1000-7210.2018.02.014.
- Carcione, J.M., 2000. A model for seismic velocity and attenuation in petroleum source rocks. Geophysics 65 (4), 1080–1092. https://doi.org/10.1190/1.1444801.
- Carcione, J.M., 2001. AVO effects of a hydrocarbon source-rock layer. Geophysics 66 (2), 419–427. https://doi.org/10.1190/1.1444933.
- Carcione, J.M., Helle, H.B., Avseth, P., 2011. Source-rock seismic-velocity models: Gassmann versus backus. Geophysics 76 (5), N37–N45. https://doi.org/10.1190/geo2010-0258.1.
- Carcione, J.M., Avseth, P., 2015. Rock-physics templates for clay-rich source rocks RPTs for clay-rich source rocks. Geophysics 80 (5), D481—D500. https://doi.org/ 10.1190/geo2014-0510.1.
- Chen, S., Zhao, W.Z., Zeng, Q.C., Yang, Q., He, P., Gai, S.H., Deng, Y., 2018. Quantitative prediction of TOC content in shale gas reservoirs using seismic data: a case study from the Lower Silurian Longmaxi Formation in the Chang Ning gas field of the Sichuan Basin. China. Interpretation 5 (1), 1–40. https://doi.org/10.1190/INT-2018-0038.1.
- Chen, X.Y., Wang, F.L., Li, H.Y., Yin, J., Xie, M.J.S., Cao, Y.J., 2021. Differential oil accumulation and its controlling factors for CFD6-4 oilfield at the steep slope belt on the southern margin of Shijiutuo Uplift in Bohai Sea. Mar. Petrol. Geol. 133, 105266. https://doi.org/10.1016/j.marpetgeo.2021.105266.
- Chen, Z.Q., 2014. Quantitative seismic prediction technique of marine shale TOC and its application: a case from the Longmaxi Shale Play in the Jiaoshiba area, Sichuan Basin. Nat. Gas. Ind. 34 (6), 24–29. https://doi.org/10.3787/j.issn.1000-0976.2014.06.004.
- Chopra, S., Sharma, R.K., Nemati, H., Keay, J., 2018. Seismic reservoir characterization of Utica-Point Pleasant Shale with efforts at quantitative interpretation—a case study: Part 1. Interpretation 6 (2), T313—T324. https://doi.org/10.1190/INT-2017-0134.1.
- Del Monte, A.A., Antonielli, E., De Tomasi, V., Luchetti, G., Paparozzi, E., Gambacorta, G., 2018. Methods for source rock identification on seismic data: an example from the Tanezzuft Formation (Tunisia). Mar. Petrol. Geol. 91, 108–124. https://doi.org/10.1016/j.marpetgeo.2017.12.015.
- Del Moro, Y., Anantharamu, V., Vernik, L., Quaglia, A., Carrillo, E., 2020. Seismic petrophysics workflow applied to Delaware Basin. Interpretation 8 (2), T349–T363. https://doi.org/10.1190/INT-2019-0157.1.
- Feng, Y.L., Jiang, S., Hu, S.Y., Li, S.T., Lin, C.S., Xie, X.N., 2016. Sequence stratigraphy and importance of syndepositional structural slope-break for architecture of Paleogene syn-rift lacustrine strata, Bohai Bay Basin. E. China. Mar. Petrol. Geol. 69, 183–204. https://doi.org/10.1016/j.marpetgeo.2015.10.013.
- Fu, C., Li, S.L., Li, S.L., Xu, J.Y., 2022. Tectonostratigraphic evolution of a rift basin and corresponding source-to-sink systems: implications for the western Bohai Bay Basin, North China. Mar. Petrol. Geol. 139, 105587. https://doi.org/10.1016/ j.marpetgeo.2022.105587.
- Gupta, N., Sarkar, S., Marfurt, K.J., 2013. Seismic attribute driven integrated characterization of the woodford shale in west-central Oklahoma characterization of the woodford shale. Interpretation 1 (2), SB85—SB96. https://doi.org/10.1190/INT-2013-0033.1.
- Hakimi, M.H., Ahmed, A.F., 2016. Organic-geochemistry characterization of the Paleogene to Neogene source rocks in the Sayhut subbasin, Gulf of Aden Basin, with emphasis on organic-matter input and petroleum-generation potential. AAPG Bull. 100 (11), 1749–1774. https://doi.org/10.1306/05241615201.
- Hampson, D.P., Russell, B.H., Bankhead, B., 2005. Simultaneous inversion of prestack seismic data. In: SEG Technical Program Expanded Abstracts 2005.

Society of Exploration Geophysicists, pp. 1633-1637. https://doi.org/10.1190/12148008

- Hansen, J.A., Mondol, N.H., Fawad, M., 2019. Organic content and maturation effects on elastic properties of source rock shales in the Central North Sea. Interpretation 7 (2), T477—T497. https://doi.org/10.1190/INT-2018-0105.1.
- Hao, F., Zhou, X.H., Zhu, Y.M., Zou, H.Y., Yang, Y.Y., 2010. Charging of oil fields surrounding the Shaleitian uplift from multiple source rock intervals and generative kitchens, Bohai Bay basin, China. Mar. Petrol. Geol. 27 (9), 1910–1926. https://doi.org/10.1016/j.marpetgeo.2010.07.005.
- Hao, F., Zhou, X.H., Zhu, Y.M., Yang, Y.Y., 2011. Lacustrine source rock deposition in response to co-evolution of environments and organisms controlled by tectonic subsidence and climate, Bohai Bay Basin. China. Org. Geochem. 42 (4), 323–339. https://doi.org/10.1016/j.orggeochem.2011.01.010.
- Herron, S.L., 1988. Source rock evaluation using geochemical information from wireline logs and cores (abs). AAPG Bull. 72, 1007.
- Hu, H.T., Liu, C., Lu, S.F., 2015. The method and application of using generalized-ΔLgR technology to predict the organic carbon content of continental deep source rocks. Acta Geol. Sin.-Engl. Ed. 89 (S1), 393–394. https://doi.org/10.1111/ 1755-6724 12306 14
- Huang, Z.H., Williamson, M.A., 1996. Artificial neural network modelling as an aid to source rock characterization. Mar. Petrol. Geol. 13 (2), 277–290. https://doi.org/ 10.1016/0264-8172(95)00062-3.
- Infante-Paez, L., Cardona, L.F., McCullough, B., Slatt, R., 2017. Seismic analysis of paleotopography and stratigraphic controls on total organic carbon: rich sweet spot distribution in the Woodford Shale, Oklahoma, USA. Interpretation 5 (1), T33—T47. https://doi.org/10.1190/INT-2015-0151.1.
- Ji, S.C., Yang, X.H., Zhu, H.T., Deng, Y.H., Kang, H.Q., Wang, B., 2018. Geophysical quantitative prediction of TOC content in source rocks of madingo Formation in Block A, lower Congo basin. Oil Geophys. Prospect. 53 (2), 369–380. https:// doi.org/10.13810/j.cnki.issn.1000-7210.2018.02.019.
- Jiang, F.J., Pang, X.Q., Bai, J., Zhou, X.H., Li, J.P., Guo, Y.H., 2016. Comprehensive assessment of source rocks in the Bohai Sea area, eastern China. AAPG Bull. 100 (6), 969–1002. https://doi.org/10.1306/02101613092.
- Jiang, X., Liu, L.F., Sun, H.F., Huang, S.B., Geng, M.Y., Chen, S.P., Li, N., Shen, P., 2019. Differential distribution of high-quality lacustrine source rocks controlled by climate and tectonics: a case study from Bozhong sag. Acta Pet. Sin. 40 (2), 165. https://doi.org/10.7623/syxb201902004.
- Kamali, M.R., Mirshady, A.A., 2004. Total organic carbon content determined from well logs using ΔLogR and Neuro Fuzzy techniques. J. Petrol. Sci. Eng. 45 (3–4), 141–148. https://doi.org/10.1016/j.petrol.2004.08.005.
- Kenomore, M., Hassan, M., Dhakal, H., Shah, A., 2017. Total organic carbon evaluation of the bowland shale Formation in the upper bowland of the widmerpool gulf. J. Petrol. Sci. Eng. 150, 137–145. https://doi.org/10.1016/j.petrol.2016.11.040.
- Li, H.Y., Niu, C.M., Xu, P., Liu, Q.S., Zhang, X., Cui, H.Z., 2021a. Discovery of Bozhong 13-2 Archean large monoblock volatile buried hill oilfield and its oil and gas exploration significance. Nat. Gas. Ind. 8 (4), 376–383. https://doi.org/10.3787/ i.issn.1000-0976.2021.02.003.
- Li, S., Zhu, H.T., Yang, X.H., Xu, C.G., 2021b. Seismic geomorphology, architecture and genesis of unusual confined and semiconfined sedimentary units on the northern slope of the Bonan uplift, Bohai Bay Basin, China. J. Petrol. Sci. Eng. 196, 107696. https://doi.org/10.1016/j.petrol.2020.107696.
- Li, S.F., Xu, S.H., Xue, L., Liu, X.X., Yuan, C.P., 2014. Source rock organic carbon prediction with geophysical approach in the sparsely-drilled area: a case study of Enping Depression, the Pearl Mouth Basin. Oil Geophys. Prospect. 49 (2), 369–374. https://doi.org/10.13810/j.cnki.issn.1000-7210.2014.02.022.
- Li, Y.C., Huang, Z.J., Zhang, G.C., 2001. Evaluation of the lower dongying source and oil source research in Bozhong Depression. Acta Pet. Sin. 22 (2), 44. https://doi.org/10.7623/syxb200102008.
- Liu, C., Lu, S.F., Xue, H.T., 2014. Variable-coefficient ΔlogR model and its application in shale organic evaluation. Prog. Geophys. 29 (1), 312–317. https://doi.org/ 10.6038/pg20140144.
- Liu, C., Zhao, W.C., Sun, L.D., Zhang, Y., Chen, X.H., Li, J.J., 2021. An improved ΔlogR model for evaluating organic matter abundance. J. Petrol. Sci. Eng. 206, 109016. https://doi.org/10.1016/j.petrol.2021.109016.
- Løseth, H., Wensaas, L., Gading, M., Duffaut, K., Springer, M., 2011. Can hydrocarbon source rocks be identified on seismic data? Geology 39 (12), 1167—1170. https:// doi.org/10.1130/G32328.1.
- Magoon, L.B., Dow, W.G., 1991. The petroleum system—from source to trap. AAPG Mem 60, 3–24.
- Mahmood, M.F., Ahmad, Z., Ehsan, M., 2018. Total organic carbon content and total porosity estimation in unconventional resource play using integrated approach through seismic inversion and well logs analysis within the Talhar Shale, Pakistan. J. Nat. Gas Sci. Eng. 52, 13–24. https://doi.org/10.1016/j.jngse.2018.01.016.
- Matava, T., Keys, R.G., Ohm, S.E., Volterrani, S., 2021. Observing maturing source rocks on seismic reflection data Observing source rocks on seismic data. Geophysics 86 (1), MR67–MR79. https://doi.org/10.1190/geo2020-0205.1.
- Mavko, G., Mukerji, T., Dvorkin, J., 2020. The Rock Physics Handbook, 3nd ed. Cambridge university press. https://doi.org/10.1017/9781108333016.
- Mendelzon, J.D., Toksoz, M.N., 1985. Source rock characterization using multivariate analysis of log data. In: SPWLA 26th Annual Logging Symposium. Dallas, Texas, USA, June 17-20.
- Meyer, B.L., Nederlof, M.H., 1984. Identification of source rocks on wireline logs by density/resistivity and sonic transit time/resistivity crossplots. AAPG Bull. 68

- (2), 121–129. https://doi.org/10.1306/AD4609E0-16F7-11D7-8645000102C1865D.
- Niu, C., Liu, Z.B., Wang, Y.C., Zhang, Y.M., Xie, J.G., Huang, R., 2017. Quantitative evaluation of Shahejie formation source rocks in Liaoxi Sag with geophysical approaches. Oil Geophys. Prospect. 52 (1), 131–137. https://doi.org/10.13810/ j.cnki.issn.1000-7210.2017.01.018.
- Paris, A.G., Stewart, R.R., 2020. Predicting reservoir quality in the Bakken Formation, North Dakota, using petrophysics and 3C seismic data. Interpretation 8 (4), T851—T868. https://doi.org/10.1190/INT-2020-0007.1.
- Passey, Q., Creaney, S., Kulla, J., Moretti, F., Stroud, J., 1990. A practical model for organic richness from porosity and resistivity logs. AAPG Bull. 74 (12), 1777–1794. https://doi.org/10.1306/0C9B25C9-1710-11D7-8645000102C1865D.
- Peters, K.E., 1986. Guidelines for evaluating petroleum source rock using programmed pyrolysis. AAPG Bull. 70 (3), 318–329. https://doi.org/10.1306/94885688-1704-11D7-8645000102C1865D.
- Qi, J.F., Zhang, Y.W., Lu, K.Z., Yang, Q., 1995a. Cenozoic tectonic evolution in Bohai Bay Basin province. J. Univ. Petrol., China 19 (Suppl. I), 1–6. Qi, J.F., Zhang, Y.W., Lu, K.Z., Yang, Q., Chen, F.J., 1995b. Extensional pattern and
- Qi, J.F., Zhang, Y.W., Lu, K.Z., Yang, Q., Chen, F.J., 1995b. Extensional pattern and dynamic process of the Cenozoic rifting basin in the Bohai Bay. Exp. Pet. Geol. 17, 316–323. https://doi.org/10.11781/sysydz199504316.
- Qin, J.Q., Fu, D.L., Qian, Y.F., Yang, F., Tian, T., 2018. Progress of geophysical methods for the evaluation of TOC of source rock. Geophys. Prospect. Pet. 57, 803–812. https://doi.org/10.3969/j.issn.1000-1441.2018.06.002.
- Sahoo, T.R., Funnell, R.H., Brennan, S.W., Sykes, R., Thrasher, G.P., Adam, L., Lawrence, M.J., Kellett, R.L., Ma, X., 2021. Delineation of coaly source rock distribution and prediction of organic richness from integrated analysis of seismic and well data. Mar. Petrol. Geol. 125, 104873. https://doi.org/10.1016/i.marpetgeo.2020.104873.
- Schmoker, J.W., 1981. Determination of organic-matter content of Appalachian Devonian shales from gamma-ray logs. AAPG Bull. 65 (7), 1285–1298. https://doi.org/10.1306/03859494-16D1-11D7-8645000102C1865D.
- Schmoker, J.W., Hester, T.C., 1983. Organic carbon in Bakken formation, United States portion of Williston basin. AAPG Bull. 67 (12), 2165—2174. https://doi.org/ 10.1306/AD460931-16F7-11D7-8645000102C1865D.
- Sêco, S.L., Silva, R.L., Watson, N., Duarte, L.V., Pereira, A.J., Wach, G., 2019. Application of petrophysical methods to estimate total organic carbon in Lower Jurassic source rocks from the offshore Lusitanian Basin (Portugal). J. Petrol. Sci. Eng. 180, 1058–1068. https://doi.org/10.1016/j.petrol.2019.05.065.
- Sen, M.K., Stoffa, P.L., 2013. Global Optimization Methods in Geophysical Inversion. Cambridge University Press. https://doi.org/10.1017/CB09780511997570.
- Shalaby, M.R., Jumat, N., Lai, D., Malik, O., 2019. Integrated TOC prediction and source rock characterization using machine learning, well logs and geochemical analysis: case study from the Jurassic source rocks in Shams Field, NW Desert, Egypt. J. Petrol. Sci. Eng. 176, 369–380. https://doi.org/10.1016/ j.petrol.2019.01.055.
- Shi, H.S., Wang, Q.B., Wang, J., Liu, X.J., Feng, C., Hao, Y.W., Pan, W.J., 2019. Discovery and exploration significance of large condensate gas fields in BZ19-6 structure in deep Bozhong sag. China Pet. Explor. 24 (1), 36. https://doi.org/10.3969/ j.issn.1672-7703.2019.01.005.
- Shi, H.S., Niu, C.M., Hou, M.C., Gao, Y.D., Lai, W.C., Chen, A.Q., Xu, G.S., Xu, P., Cao, H.Y., Yan, J.G., 2021. Analysis of hydrocarbon accumulation conditions of double-layered Archaeozoic buried hill and major discovery of Bozhong 13-2 Oil and Gasfield, Bohai sea area. China Pet. Explor. 26 (2), 12. https://doi.org/10.3969/j.issn.1672-7703.2021.02.002.
- Sun, Y.H., Qi, J.F., Lv, Y.F., Han, H.J., 2008. Characteristics of fault structure and its control to hydrocarbon in Bozhong Depression. Acta Pet. Sin. 29 (5), 669–675. https://doi.org/10.7623/syxb200805007.
- Swanson, V.E., 1960. Oil Yield and Uranium Content of Black Shales. USGS Professional Paper 356-A, pp. 1–47.
- Tan, M.J., Song, X.D., Yang, X., Wu, Q.Z., 2015. Support-vector-regression machine technology for total organic carbon content prediction from wireline logs in organic shale: a comparative study. J. Nat. Gas Sci. Eng. 26, 792–802. https:// doi.org/10.1016/j.jngse.2015.07.008.
- Tao, Q.Q., Li, D., Yang, X.B., Hu, L., Xu, X.D., 2015. Hydrocarbon source rock prediction with frequency-divided inversion. Oil Geophys. Prospect. 50 (4), 706–713. https://doi.org/10.13810/j.cnki.issn.1000-7210.2015.04.019.
- Tenaglia, M., Eberli, G.P., Weger, R.J., Blanco, L.R., Sánchez, L.E.R., Swart, P.K., 2020. Total organic carbon quantification from wireline logging techniques: a case study in the Vaca Muerta Formation, Argentina. J. Petrol. Sci. Eng. 194, 107489. https://doi.org/10.1016/j.petrol.2020.107489.
- Tissot, B.P., 1984. Recent advances in petroleum geochemistry applied to hydrocarbon exploration. AAPG Bull. 68 (5), 545–563. https://doi.org/10.1306/AD461336-16F7-11D7-8645000102C1865D.
- Tissot, B.P., Pelet, R., Ungerer, P.H., 1987. Thermal history of sedimentary basins, maturation indices, and kinetics of oil and gas generation. AAPG Bull. 71 (12), 1445–1466. https://doi.org/10.1306/703C80E7-1707-11D7-8645000102C1865D.
- Verma, S., Zhao, T., Marfurt, K.J., Devegowda, D., 2016. Estimation of total organic carbon and brittleness volume. Interpretation 4 (3), T373—T385. https://doi.org/10.1190/INT-2015-0166.1.
- Vernik, L., Nur, A., 1992. Ultrasonic velocity and anisotropy of hydrocarbon source rocks. Geophysics 57 (5), 727–735. https://doi.org/10.1190/1.1443286.
- Vernik, L., Landis, C., 1996. Elastic anisotropy of source rocks: implications for hydrocarbon generation and primary Migration. AAPG Bull. 80 (4), 531–544. https://doi.org/10.1306/64ED8836-1724-11D7-8645000102C1865D.

Wang, G.M., Xiong, Z.H., Zhang, J., Guo, Y.H., Lin, G.S., Fu, Y., 2017. Characterization of fault system and its control on reservoirs in the Bozhong sag, Bohai Bay Basin. Oil Gas Geol. 38 (1), 62–70. https://doi.org/10.11743/ogg20170107.

- Wang, H.J., Wu, W., Chen, T., Dong, X.J., Wang, G.X., 2019. An improved neural network for TOC, S₁ and S₂ estimation based on conventional well logs. J. Petrol. Sci. Eng. 176, 664–678. https://doi.org/10.1016/j.petrol.2019.01.096.
- Wang, J., Shi, W.Z., Shu, Z.G., Xu, Q.H., Zhang, X.M., Xu, Z., 2016a. TOC content quantitative prediction in organic-rich shale. Oil Geophys. Prospect. 51 (3), 596–604. https://doi.org/10.13810/j.cnki.issn.1000-7210.2016.03.023.
- Wang, M., Wilkins, R.W., Song, G.Q., Zhang, L.Y., Xu, X.Y., Li, Z., Chen, G.H., 2015. Geochemical and geological characteristics of the Es3L lacustrine shale in the Bonan sag, Bohai Bay Basin, China. Int. J. Coal Geol. 138, 16–29. https://doi.org/ 10.1016/i.coal.2014.12.007.
- Wang, P., Peng, S., 2018. A new scheme to improve the performance of artificial intelligence techniques for estimating total organic carbon from well logs. Energies 11 (4), 747. https://doi.org/10.3390/en11040747.
- Wang, P.W., Chen, Z.H., Pang, X.Q., Hu, K.Z., Sun, M.L., Chen, X., 2016b. Revised models for determining TOC in shale play: example from Devonian Duvernay shale, Western Canada sedimentary basin. Mar. Petrol. Geol. 70, 304–319. https://doi.org/10.1016/j.marpetgeo.2015.11.023.
- Wang, Q., Hao, F., Xu, C.G., Zou, H.Y., 2020. Paleolimnological environments and the formation of high quality source rocks in the Bohai Bay Basin: an integrated geochemical study of biomarkers, stable carbon and oxygen isotopes, and trace elements. J. Petrol. Sci. Eng. 195, 107753. https://doi.org/10.1016/ j.petrol.2020.107753.
- Wang, Q., Hao, F., Xue, Y.A., Niu, C.M., Zou, H.Y., Yin, J., Miao, Q.Y., Liu, M.X., 2022a. Geochemistry and origin of the Bozhong 19-6 condensates: implications for deep gas accumulation in the Bohai Bay Basin. AAPG Bull. 106 (4), 869–896. https://doi.org/10.1306/10042120106.
- Wang, X., Ma, J.F., Wang, F.L., Wang, Z.L., Chen, R.T., Yan, X.Y., 2022b. Prediction of organic facies of deep source rocks in southwestern part of Bozhong Sag, Bohai Bay Basin. Exp. Pet. Geol. 44 (6), 1070–1080. https://doi.org/10.11781/svsvdz2022061070.
- Watson, M.P., Hayward, A.B., Parkinson, D.N., Zhang, Z.M., 1987. Plate tectonic history, basin development and petroleum source rock deposition onshore China. Mar. Petrol. Geol. 4 (3), 205–225. https://doi.org/10.1016/0264-8172(87)90045-6
- Xie, Y.H., Zhang, G.C., Shen, P., Liu, L.F., Huang, S.B., Chen, S.P., Yang, S.C., 2018. Formation conditions and exploration direction of large gas field in Bozhong sag of Bohai Bay Basin. Acta Pet. Sin. 39 (11), 1199. https://doi.org/10.7623/ svxb201811001.

- Xu, C.G., Yu, H.B., Wang, J., Liu, X.J., 2019. Formation conditions and accumulation characteristics of Bozhong 19-6 large condensate gas field in offshore Bohai Bay Basin. Petrol. Explor. Dev. 46 (1), 27–40. https://doi.org/10.1016/S1876-3804(19) 30003-5
- Xue, Y.A., Wang, Q., Niu, C.M., Miao, Q.Y., Liu, M.X., Yin, J., 2020. Hydrocarbon charging and accumulation of BZ 19-6 gas condensate field in deep buried hills of Bozhong depression, Bohai Sea. Oil Gas Geol. 41 (5), 891–902. https://doi.org/10.11743/ogg20200501.
- Yin, J., Xu, C.G., Hao, F., Wang, Q., Miao, Q.Y., Wang, Z.Q., Zou, H.Y., 2020. Controls on organic matter enrichment in source rocks of the Shahejie Formation in the southwestern Bozhong sag, Bohai Bay Basin, China. Paleogeogr. Paleoclimatol. Paleoecol. 560, 110026. https://doi.org/10.1016/j.palaeo.2020.110026.
- Yu, Y.X., Zhou, X.H., Xu, C.G., Wu, K., Lv, D.Y., Liu, Y.B., Zhou, X., 2020. Architecture and evolution of the Cenozoic offshore Bohai Bay basin, eastern China. J. Asian Earth Sci. 192, 104272. https://doi.org/10.1016/j.jseaes.2020.104272.
- Zhang, H., Zhu, G.Y., 2007. Using seismic and log information to predict and evaluate hydrocarbon source rocks: an example from rich oil depressions in Bohai Bay. Petrol. Explor. Dev. 34 (1), 55–59.
- Zhao, L.X., Wang, Y., Liu, X.W., Zhang, J.Q., Liu, Y.W., Qin, X., Li, K.J., Geng, J.H., 2020. Depositional impact on the elastic characteristics of the organic shale reservoir and its seismic application: a case study of the Longmaxi-Wufeng Shale in the Fuling gas field, Sichuan Basin. Geophysics 85 (2), B23–B33. https://doi.org/10.1190/geo2019-0326.1.
- Zhao, L.X., Liu, J.S., Yao, Y.X., Zhong, K., Ma, J.Q., Zou, C.F., Chen, Y.Y., Fu, X.W., Zhu, X.J., Zhu, W.L., Geng, J.H., 2021. Quantitative seismic characterization of source rocks in lacustrine depositional setting using the random forest method: an example from the Changiiang Sag in East China Sea Basin. Chin. J. Geophys. 64 (2), 700–715. https://doi.org/10.6038/cjg202100123.
- Zhao, P.Q., Mao, Z.Q., Huang, Z.H., Zhang, C., 2016. A new method for estimating total organic carbon content from well logs. AAPG Bull. 100 (8), 1311–1327. https://doi.org/10.1306/02221615104.
- Zhou, X.H., Niu, C.M., Teng, C.Y., 2009. Relationship between faulting and hydrocarbon pooling during the Neotectonic movement around the central Bohai Bay. Oil Gas Geol. 30 (4), 469–475. https://doi.org/10.11743/ogg20090413.
- Zhu, G.Y., Jin, Q., 2002. Study on source rock heterogeneity-a case of Niu-38 well in Dongying Depression. Acta Pet. Sin. 23 (5), 34–39. https://doi.org/10.7623/syxh200205007
- Zhu, L.Q., Zhang, C.M., Zhang, Z.S., Zhou, X.Q., Liu, W.N., 2019. An improved method for evaluating the TOC content of a shale formation using the dual-difference \(\Delta\text{olgR} \) method. Mar. Petrol. Geol. 102, 800—816. https://doi.org/10.1016/j.marpetgeo.2019.01.031.